Metabolic rerouting via *SCD1* induction impacts X-linked adrenoleukodystrophy

Quentin Raas,[1] Malu-Clair van de Beek,[2] Sonja Forss-Petter,[3] Inge M.E. Dijkstra,[2] Abigail Deschiffart,[1] Briana C. Freshner,[1] Tamara J. Stevenson,[1] Yorrick R.J. Jaspers,[2] Liselotte Nagtzaam,[2] Ronald J.A. Wanders,[2] Michel van Weeghel,[2] Joo-Yeon Engelen-Lee,[4] Marc Engelen,[5] Florian Eichler,[6] Johannes Berger,[3] Joshua L. Bonkowsky,[1] and Stephan Kemp[2,5]

[1]Department of Pediatrics, University of Utah, Brain and Spine Center, Primary Children's Hospital, Salt Lake City, Utah, USA. [2]Laboratory Genetic Metabolic Diseases, Department of Clinical Chemistry, Amsterdam UMC, Amsterdam Gastroenterology & Metabolism, University of Amsterdam, Amsterdam, Netherlands. [3]Department of Pathobiology of the Nervous System, Center for Brain Research, Medical University of Vienna, Vienna, Austria. [4]Department of Neurology, Amsterdam UMC, Amsterdam Neuroscience, University of Amsterdam, Amsterdam, Netherlands. [5]Department of Pediatric Neurology, Amsterdam UMC, Amsterdam Leukodystrophy Center, Emma Children's Hospital, Amsterdam Neuroscience, University of Amsterdam, Amsterdam, Netherlands. [6]Massachusetts General Hospital, Harvard Medical School, Boston, USA.

X-linked adrenoleukodystrophy (ALD) is a progressive neurodegenerative disease caused by mutations in *ABCD1*, the peroxisomal very long–chain fatty acid (VLCFA) transporter. ABCD1 deficiency results in accumulation of saturated VLCFAs. A drug screen using a phenotypic motor assay in a zebrafish ALD model identified chloroquine as the top hit. Chloroquine increased expression of stearoyl-CoA desaturase-1 (*scd1*), the enzyme mediating fatty acid saturation status, suggesting that a shift toward monounsaturated fatty acids relieved toxicity. In human ALD fibroblasts, chloroquine also increased SCD1 levels and reduced saturated VLCFAs. Conversely, pharmacological inhibition of SCD1 expression led to an increase in saturated VLCFAs, and CRISPR knockout of *scd1* in zebrafish mimicked the motor phenotype of ALD zebrafish. Importantly, saturated VLCFAs caused ER stress in ALD fibroblasts, whereas monounsaturated VLCFA did not. In parallel, we used liver X receptor (LXR) agonists to increase SCD1 expression, causing a shift from saturated toward monounsaturated VLCFA and normalizing phospholipid profiles. Finally, *Abcd1⁻/ʸ* mice receiving LXR agonist in their diet had VLCFA reductions in ALD-relevant tissues. These results suggest that metabolic rerouting of saturated to monounsaturated VLCFAs may alleviate lipid toxicity, a strategy that may be beneficial in ALD and other peroxisomal diseases in which VLCFAs play a key role.

Introduction

X-linked adrenoleukodystrophy (ALD) is a neurometabolic disease caused by mutations in the *ABCD1* gene encoding the peroxisomal CoA-activated very long–chain fatty acid (VLCFA) (≥C22:0; refs. 1–3). Mutations in *ABCD1* cause deficient peroxisomal VLCFA β-oxidation (4) and resultant VLCFA accumulation in plasma and tissues (5, 6), including the spinal cord, brain white matter, and adrenal cortex (7, 8).

ALD is characterized by a striking and unpredictable clinical spectrum, even within families (9). In childhood, around 50% of affected males develop primary adrenal insufficiency before the age of 10 (10, 11) and 30% to 35% of affected males develop a fatal cerebral inflammatory disease (cerebral ALD) (9, 12). If diagnosed in an early stage, cerebral ALD can be halted or reversed by hematopoietic stem cell transplantation (HSCT) (13, 14). In adulthood, virtually all male patients and more than 80% of affected women develop a chronic progressive myelopathy (15, 16) for which no disease-modifying therapy is available (9). Furthermore, patients who received HSCT during childhood still develop myelopathy in adulthood (17). This indicates that HSCT only stops the inflammatory component of the disease without addressing the underlying biochemical or cellular defects (17). Therefore, there is a need to develop effective treatments aimed at preventing the toxicity associated with elevated VLCFA levels in the CNS.

However, the mechanism by which elevated VLCFAs lead to disease pathology has been difficult to determine. Three models have been considered. The first is elevated fatty acid levels; however, trials of VLCFA-lowering compounds have failed to improve clinical outcomes (17). While overall serum levels of VLCFAs do not predict disease progression or disease severity, it is not known whether this is in part because of insufficient penetrance of the CNS of the compounds. The second model is fatty acid–chain length; chain length correlates with lipid toxicity. For example, injection of C24:0-lysophosphatidylcholine (C24:0-LPC), but not C16:0-LPC (C16:0-LPC) into mouse brain resulted in widespread microglial activation and apoptosis (18, 19). While

inhibition of the VLCFA-specific elongase ELOVL1 was effective in ALD fibroblasts in lowering VLCFA levels (20–22), the same effect was not seen in patients.

The third model is saturation status; the structure and function of VLCFAs depends on whether they are saturated or monounsaturated fatty acids. Exposure of ALD fibroblasts to saturated VLCFAs (C26:0) resulted in a 16-fold increase in endoplasmic reticulum (ER) stress marker XBP1, whereas exposure to the monounsaturated VLCFA C26:1 caused only a 1.3-fold increase (23). This is in line with earlier reports showing that addition of oleic acid (C18:1, monounsaturated) can even halt ER stress that was induced by high levels of palmitic acid (C16:0, saturated) (24). In ALD patient fibroblasts, saturated VLCFAs induce oxidative stress (25), mitochondrial dysfunction (25–27), and ER stress (23, 28). Saturation status is regulated by stearoyl-CoA desaturase-1 (SCD1), which catalyzes the synthesis of monounsaturated fatty acids by the introduction of a *cis* double bond at the Δ-9 position of C16:0 or C18:0, giving rise to C16:1 and C18:1, respectively (29). These findings suggest that saturation status of VLCFAs may be central to the toxic effects of VLCFAs and that promoting desaturation could be beneficial for ALD.

However, functional demonstration of a beneficial effect from modulating fatty acid saturation status has been wanting. The *Abcd1*-deficient mouse, which develops impaired motor function and spinal cord involvement with similarity to the human adrenomyelopathy (AMN) variant of ALD, does not start to develop a phenotype until after age 15 months, limiting assessment of therapeutic interventions and other manipulations (30, 31). A new tool for studies of ALD was provided through generation of a zebrafish *abcd1* mutant model (32). The zebrafish ALD model not only recapitulates key aspects of ALD, but also manifests a motor phenotype in the first week of life. Importantly, in zebrafish, the *ABCD1* DNA and protein sequences are highly conserved, as are other key genes in lipid metabolism, including *SCD1* and *ELOVL1* (32–34).

In the present study, a high-throughput small compound screen was performed using a functional motor behavior assay in the zebrafish ALD model. Characterization of chloroquine (CQ), the top hit from the screen, showed that it increased *scd1* expression, an observation confirmed in human ALD fibroblast cells. We investigated the effect of pharmacologically induced SCD1 enzyme activity on fatty acid synthesis both in ALD patient cell lines and *Abcd1⁻/y* mice. We found that activation of SCD1 caused a shift in the synthesis of saturated VLCFAs toward monounsaturated VLCFAs, decreasing levels of saturated VLCFAs in ALD human fibroblasts and mouse tissues. These results indicate that saturated VLCFAs mediate key disease pathology in ALD and suggest that metabolic rerouting toward the monounsaturated fatty acids may open a new option toward a therapy for ALD and other peroxisomal disorders.

Results

CQ rescues aberrant swimming behavior in zebrafish ALD mutants. We previously generated and characterized zebrafish *abcd1* mutants, showing that, similarly to ALD patients, they have elevated VLCFA levels (32). The mutants have aberrant CNS development, including hypomyelination in the spinal cord, abnormal patterning, and decreased numbers of oligodendrocytes, and increased cell death

in the nervous system. By day of life 5 (days post fertilization[dpf]), *abcd1* mutants demonstrate impaired motor swimming function.

We tested and validated a functional motor assay for the *abcd1* mutants. We reasoned that drug screening in zebrafish has been successfully used to identify target pathways as well as therapeutic compounds for human diseases (35–37). We screened a 2528 compound library (Microsource Spectrum) to identify drugs that rescue the motor (swimming) behavior in *abcd1* mutants (*abcd1^{sa509/sa509}*). Individual mutant animals were plated at 3 dpf into a 96-well tray and exposed to control (0.1% DMSO) or compound (groups of 4 compounds, each at 10 μm in 0.1% DMSO; 12 animals per compound group; Supplemental Figure 1; supplemental material available online with this article; https://doi.org/10.1172/JCI142500DS1) from 4 to 7 dpf. Motor assay testing was performed at 7 dpf using an automated system that tracked and recorded individual animals (Figure 1A). We found 74 compounds with a *z* score greater than 1 SD improvement in composite motor behavior (distance swum, velocity, maximum velocity, time spent moving, and active velocity) (Figure 1B and Supplemental Tables 1, 2, and 3).

We then rescreened the 18 compounds with the highest *z* scores; each drug was individually screened on 48 each *abcd1^{sa509/sa509}*, *abcd1^{sa509/+}*, or WT larvae at a dose of 2.5 μm at 3 different ages and compared with control treatment (0.1% DMSO, Figure 2A, Supplemental Figure 1, and Supplemental Figure 2). The 2 most promising compounds, prednisolone and CQ, were then individually rescreened (Figure 2B). CQ showed a dose-dependent effect that was present at different developmental stages for the 2 most significant motor assays and had a persistent effect even at 7 dpf without redosing. In the initial screen, we used the *abcd1^{sa509}* allele, but had also characterized other alleles (32). This effect of CQ was confirmed in ALD zebrafish carrying 2 different mutant alleles (*abcd1^{sa509}* and *abcd1^{zc92}*).

Increased scd1 expression found in zebrafish mutants after CQ administration. To test the mechanism by which CQ rescued ALD zebrafish behavior, we tested different potential mechanisms. CQ is known to interfere with lysosomal activity and autophagy (38); thus, we investigated the effect of bafilomycin A1, a compound known to target the lysosome V-ATPase and affect autophagy similarly. Bafilomycin A1 did not mimic the effect of CQ and could not rescue the abnormal swimming behavior of mutant fish, suggesting an alternative mechanism of action (and potentially a milder involvement of the autophagic response in this effect) (Figure 3A). In zebrafish ALD mutants, there is a decrease in the number of oligodendrocytes (32). CQ rescued the number of oligodendrocytes, as quantified using the *olig2:dsRed* transgenic reporter line in the mutant background (WT [*n* = 9], 85.0 ± 8.5 vs. *sa509/sa509* [*n* = 9], 69.1 ± 12.7, unpaired *t* test, *P* = 0.0066; and *sa509/sa509* [*n* = 9], 69.1 ± 12.7 vs. *sa509/sa509* + CQ (*n* = 8), 84.1 ± 14.5, unpaired *t* test, *P* = 0.038) (Figure 3B).

Next, we assayed expression of genes related to VLCFA synthesis and saturation status and to myelin synthesis, comparing WT and *abcd1^{sa509}* mutant larvae with or without CQ (Figure 3C). The largest effect of CQ in the ALD mutant was increased expression of *scd*, the ortholog of human *SCD1*. Of note, this change was accompanied by an increased expression of ELOVL fatty acid elongase 1b (*elovl1b*) and ELOVL fatty acid elongase 6 (*elovl6*), orthologs of the human ELOVL1 and ELOVL6 respectively, whose activities are potential modulators of VLCFA levels (20). SCD1 is an
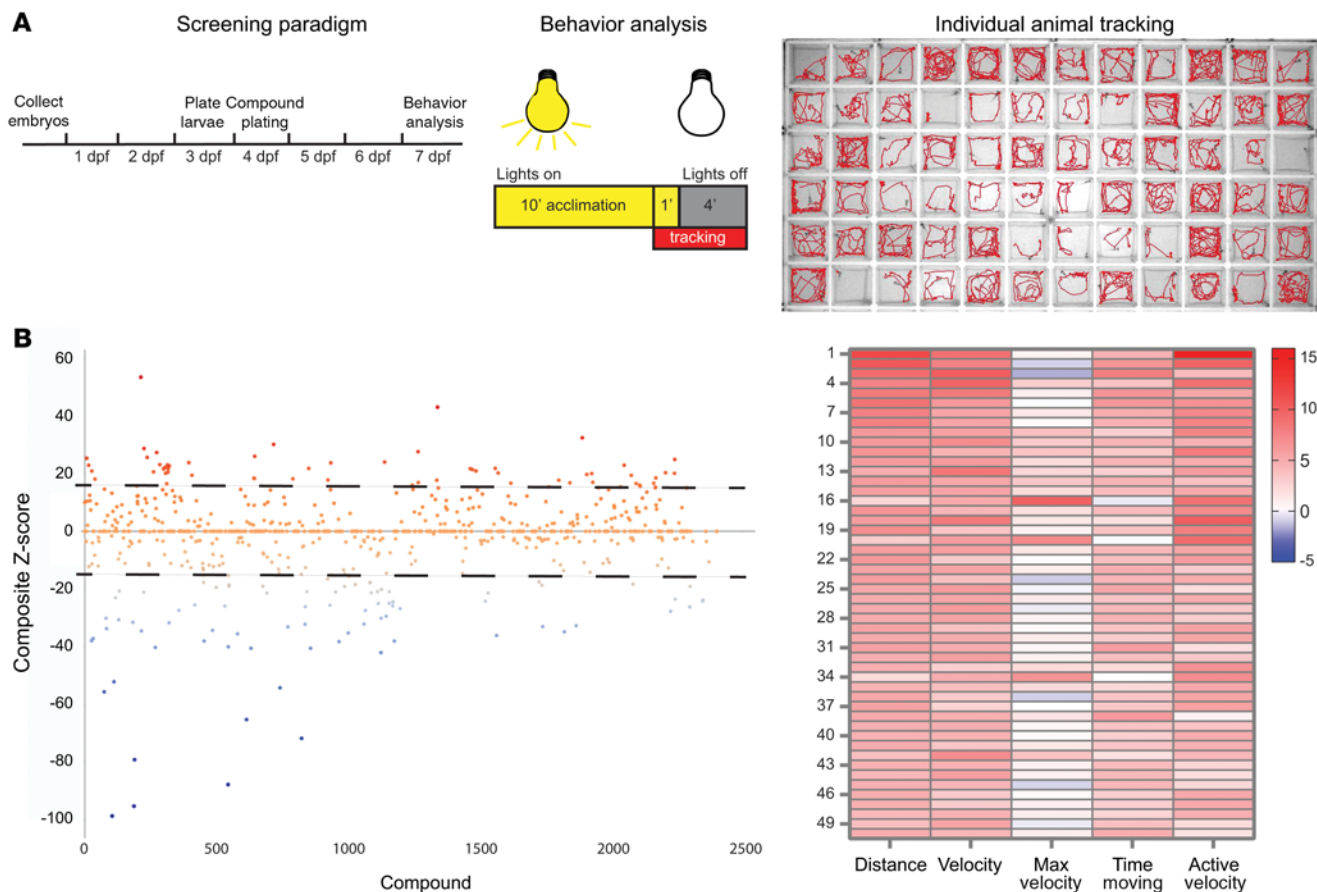
Figure 1. Zebrafish ALD mutant phenotypic drug screen; overview and primary screen. (**A**) Screen schematic. Mutant ALD zebrafish larvae (*abcd1*[sa509/sa509]) were treated from 4 to 7 dpf in 96-well trays either with control (DMSO, 0.1%) or compound (10 μm in 0.1% DMSO). Dark-evoked swimming behavior was then recorded, individual animals tracked, and data analyzed to identify compounds affecting motor behavior. Abnormal (decreased) swimming indicated by fewer tracings. (**B**) 2538 Compounds from the Microsource Spectrum library were screened; a composite z score was calculated to discriminate compounds above or below 1 SD (dotted line), and z score values for different motor behavior parameters are displayed for the top 50 compounds (heatmap). Mutant swimming behavior was set as the baseline for the z score.

iron-containing enzyme that catalyzes a rate-limiting step in the synthesis of monounsaturated fatty acids (29). Hence activation of SCD1 causes a shift from the saturated toward the monounsaturated fatty acids. In the zebrafish *abcd1* mutants, increased *scd1* expression by CQ may alleviate toxicity from saturated VLCFAs.

To test this potential role of *scd* activity in the ALD zebrafish, we used CRISPR to knock down expression of *scd* and its closely related protein paralog stearoyl-CoA desaturase b (*scdb*) (many genes in zebrafish have 2 closely related paralogs due to an ancestral duplication of large regions of the genome; ref. 39). Because CRISPR is of such high efficiency in zebrafish embryos, biallelic knockdown can be achieved (40). CRISPR disruption in injected embryos was confirmed by high-resolution melt analysis (HRMA) after PCR. We found that knockdown of *scd* and *scdb* in zebrafish larvae caused a defective swimming behavior that phenocopies the ALD mutant zebrafish (Figure 3D). However, in ALD mutant larvae, no worsening of the phenotype was observed with additional *scd* and *scdb* knockdown.

CQ reduces saturated VLCFAs in human fibroblasts. VLCFA levels are established by the balance between degradation via peroxisomal β-oxidation and synthesis through elongation of long-chain

fatty acids (LCFAs) (41). In ALD, saturated VLCFA (C26:0) levels are elevated, but C22:0 and C24:0 VLCFAs are decreased or near normal (42). To investigate the pathway underlying the elevated levels of C26:0, we had previously developed a method to measure de novo D_3-C26:0 synthesis in whole cells using 3 days of treatment with deuterium-labeled LCFA C16:0 (D_3-C16:0) (20).

We examined the impact of CQ upon de novo D_3-C26:0 synthesis from D_3-C16:0 in human control and ALD fibroblasts. As shown previously, ALD fibroblasts had increased levels of D_3-C26:0 (Figure 4A). Addition of 12.5 μm CQ reduced D_3-C26:0 levels in control fibroblasts by 75% and in ALD fibroblasts by 70%. We examined the effect of CQ on the desaturase activity of SCD1 by measuring the synthesis of D_5-C18:1 from D_5-C18:0. Addition of 12.5 μm CQ increased desaturation of D_5-C18:0 to D_5-C18:1 in controls by 20% and in ALD fibroblasts by 30% (Figure 4B). Hence, in human cells, CQ treatment resulted in a reduction in saturated VLCFA levels and also shifted fatty acids to increased monounsaturated forms.

Inhibition of SCD1 increases C26:0 synthesis. Diminished SCD1 activity has been shown to affect the accumulation, composition, and saturation status of cellular membrane phospholipids and neutral lipids (43). Given the reduction in saturated VLCFAs from CQ
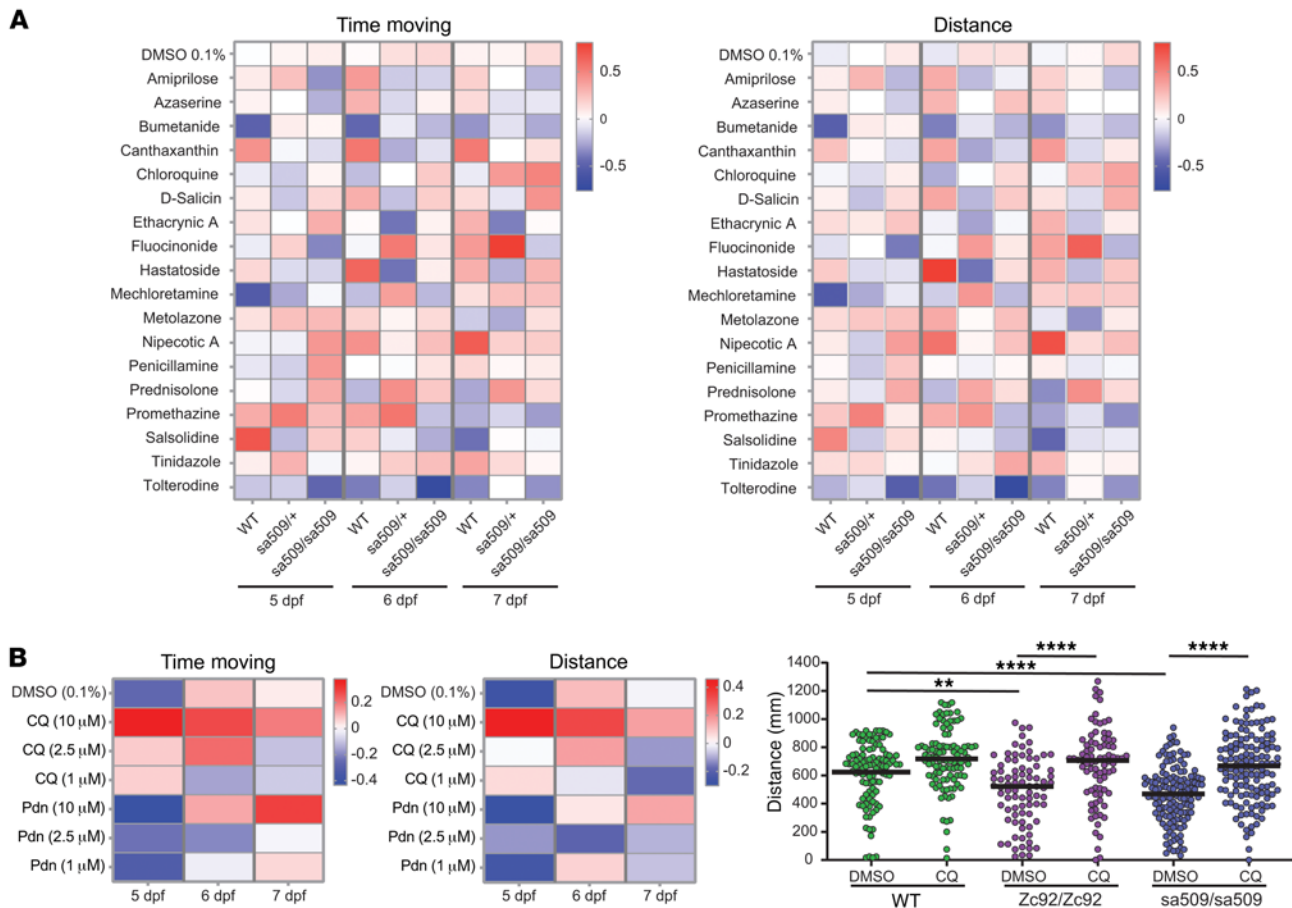
Figure 2. Zebrafish phenotypic secondary screening to identify CQ. (**A**) Heatmap of results of a secondary screen performed on the 15 compounds with the highest *z* scores, comparing control (0.1% DMSO) versus compound (2.5 μm in 0.1% DMSO) homozygous *abcd1sa509/sa509*, heterozygous *abcd1sa509/+* mutants (*n* = 48), or their WT relatives (*n* = 48). (**B**) Rescreening of the 2 top hits. Heatmap of *z* scores for distance and time-moving values of 5 to 7 dpf *abcd1sa509* mutants treated with 1, 2.5, or 10 μM CQ or prednisolone (*n* = 70–150). Right panel; effect of CQ (10 μM) on the distance swum by 7 dpf *abcd1sa509*, *abcd1zc92*, or WT larvae (*n* = 90–130 per group); 2-way ANOVA, followed by Bonferroni's multiple comparison test. ****P < 0.01; ****P < 0.0001.**

exposure, we investigated to determine whether SCD1 inhibition could specifically increase saturated VLCFAs and thereby aggravate pathology. First, we assessed the impact of the SCD1 inhibitor 4-(2-chlorophenoxy)-*N*-(3-(3-methylcarbamoyl)phenyl) piperidine-1-carboxamide (SCD1i) upon SCD1 activity and de novo VLCFA synthesis in human control and ALD fibroblasts.

Addition of 150 nM of SCD1i blocked D_5-C18:1 synthesis in both control and ALD fibroblasts by 80%. Furthermore, CQ treatment could not overcome this inhibition (Figure 4B). To determine whether CQ's effect to reduce C26:0 synthesis is mediated by increased activity of SCD1, de novo D_3-C26:0 synthesis was measured in the presence of CQ with and without SCD1i. CQ treatment reduced the synthesis of D_3-C26:0 in ALD cells by 70%. After adding 150 nM of SCD1i, the levels of D_3-C26:0 were even further elevated than in untreated ALD cells. Addition of CQ and SCD1i together largely abolished the effect of CQ on de novo D_3-C26:0 synthesis (Figure 4A).

LXR agonists increase SCD1 protein levels and activity in human fibroblasts. To remove potential confounding effects due to the multiple targets of CQ and to characterize the role of SCD1 in fatty acid pathways, we used the liver X receptor (LXR)/pan agonist TO901317, which has been shown to increase the levels of *Scd1* mRNA in mouse kidney (44). We cultured control and ALD fibroblasts with the vehicle, DMSO, or TO901317. After incubation with DMSO, only very low levels of SCD1 protein were detectable in control or ALD fibroblasts. In contrast, when control and ALD fibroblasts were incubated with 5 μM TO901317, SCD1 protein levels were markedly increased (Figure 4C). To determine whether this was a general effect of LXR agonists, we cultured control and ALD fibroblasts with GW3965, another LXR pan agonist, and LXR623, a partial LXR agonist. SCD1 protein was markedly increased after incubation with GW3965 and LXR623 in both control and ALD fibroblasts (Figure 4C).

To determine whether LXR agonist treatment is equivalent to the effects of CQ on SCD1 activity, we incubated control and ALD fibroblasts for 24 hours with D_5-C18:0 combined with DMSO (untreated), TO901317, GW3965, or LXR623 and measured the amount of D_5-C18:1 formed from D_5-C18:0 (Figure 4D). Incubation with LXR agonists resulted in a highly significant (*P* < 0.0001) increase in D_5-C18:1 levels in both control and ALD fibroblasts. To demonstrate that the increased levels of D_5-C18:1 are the result of enhanced SCD1 enzyme activity, we added SCD1i to fibroblasts and measured monounsaturated levels (analogous to CQ experiments shown in Figure 4B). In the presence of SCD1i, no increase in D_5-C18:1 synthesis was measured. Taken together, these results show that LXR
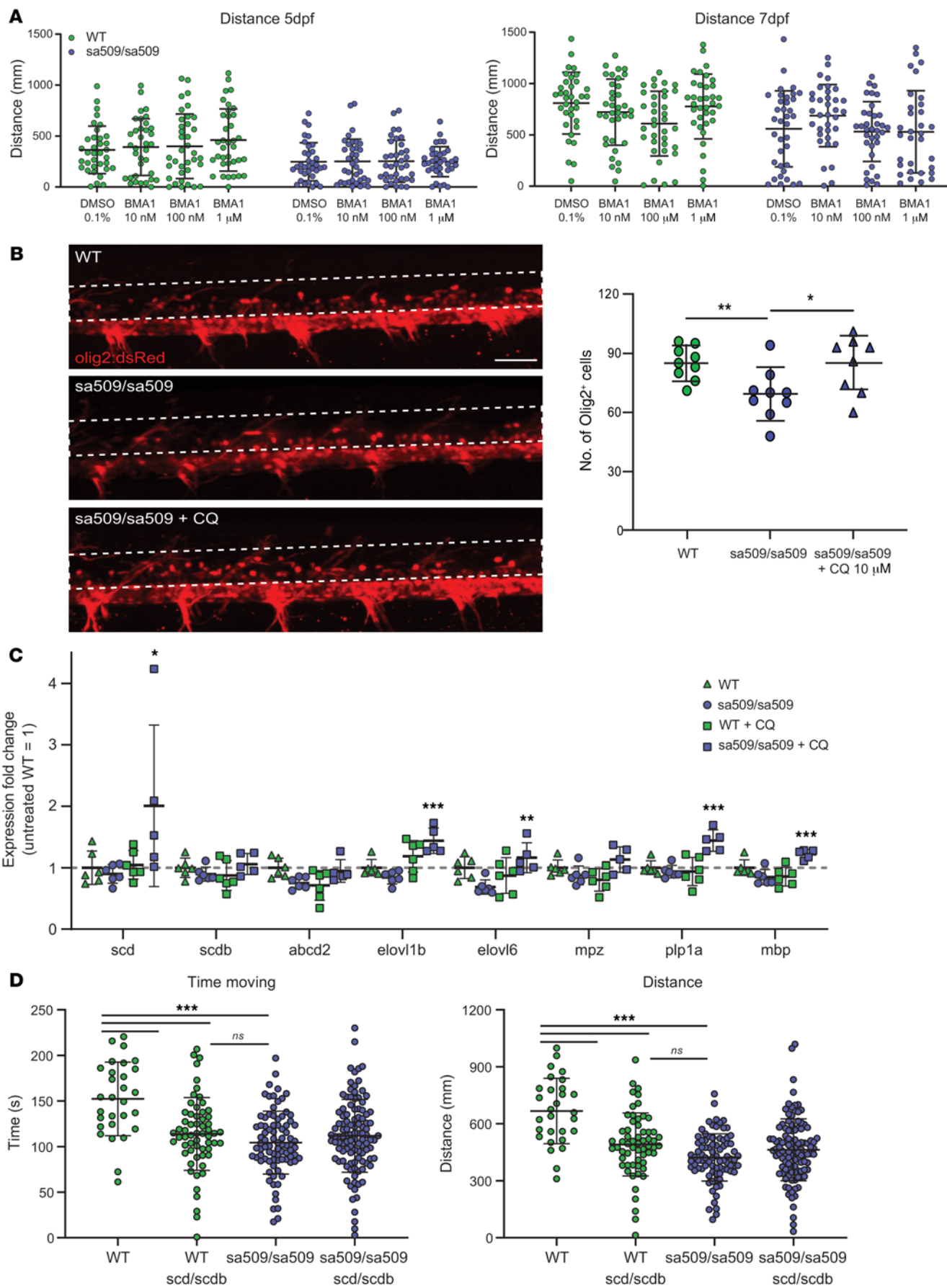
Figure 3. Characterization of CQ effects in zebrafish ALD mutant and identification of potential for mechanism via increased *scd* expression. (**A**) No effect of bafilomycin A1 (BMA1) on the motor behavior of WT or *abcd1sa509* mutant larvae. Distance moved after 24 hours of treatment (5 dpf) or 72 hours of treatment (7 dpf) with bafilomycin A1 at the indicated dose. (**B**) Effect of CQ (10 μm) on the number of Olig2+ cells in the spinal cord of 5 dpf *abcd1sa509* mutant larvae. Olig2+ cells were counted in spinal cord (region for quantification indicated by dotted line) (Z-stack confocal images of spinal cord: dorsal, top; rostral, left) using *olig2:dsRed* transgenic line in the *abcd1sa509* mutant background. Scale bar: 25 μM. (**C**) The effect of CQ (10 μm) on the expression of genes involved in fatty acid metabolism and myelin synthesis was analyzed by qRT-PCR at 7 dpf in WT or *abcd1sa509* mutant larvae (fold change of mRNA levels compared with WT control normalized to β-actin expression). *abcd2*, ATP-binding cassette transporter D2; *mpz*, myelin protein zero; *plp1a*, proteolipid protein 1a; *mbp*, myelin basic protein. (**D**) Loss of *scd* phenocopies does not worsen ALD mutant zebrafish behavior. Motor behavior of *abcd1sa509*, *scd/scdb*, and *abcd1sa509/scd/scdb* mutant 6 dpf larvae. Statistical significance by 1-way ANOVA, followed by Bonferroni's multiple comparison test. *$P < 0.05$; **$P < 0.01$; ***$P < 0.001$.

agonists increase SCD1 protein levels and thereby affect fatty acid desaturation activity in human ALD and control fibroblasts.

LXR agonists lower saturated VLCFA levels by shifting synthesis toward monounsaturated VLCFA. Next, we determined whether incubation with LXR agonists and subsequent increased fatty acid desaturation activity would lead to decreased levels of de novo synthesized C26:0 and increased levels of de novo synthesized C26:1. To this end, we incubated control and ALD fibroblasts for 3 days with D_3-C16:0 combined with the LXR agonists and measured the levels of saturated and monounsaturated VLCFA (D_3-C26:0 and D_3-C26:1, respectively) synthesized from D_3-C16:0. In ALD fibroblasts, the levels of D_3-C26:0 were significantly reduced after incubation with either TO901317, GW3965, or LXR623 ($P < 0.0001$ for all; Figure 5A). In control fibroblasts, we found no significant differences in the levels of D_3-C26:0 after incubation with the LXR agonists. This is probably due to the already low levels of D_3-C26:0 formed in control fibroblasts. Notably, the D_3-C26:0 levels in ALD fibroblasts after treatment with LXR agonists were comparable with the levels of D_3-C26:0 in control fibroblasts without LXR agonists. Inhibition of SCD1 enzymatic activity (SCDi) resulted in enhanced D_3-C26:0 synthesis and a complete block in D_3-C26:1 synthesis in ALD fibroblasts (Figure 5A). This indicates that the de novo synthesis of D_3-C26:0 was normalized in ALD fibroblasts upon incubation with LXR agonists.

As anticipated, the decrease in de novo D_3-C26:0 was accompanied by a shift toward the increased de novo synthesis of monounsaturated fatty acids. A significant increase in monounsaturated VLCFA (D_3-C26:1) levels in control and ALD fibroblasts was found upon incubation with either TO901317, GW3965, or LXR623 ($P < 0.0001$ for all; Figure 5B). Taken together, these results show that LXR agonists affect de novo VLCFA synthesis by shifting the synthesis from saturated VLCFA toward monounsaturated VLCFA.

To study how prolonged exposure of ALD fibroblasts to LXR agonists affects endogenous C26:0 levels, we cultured ALD fibroblasts for up to 3 weeks in the presence of 5 μM TO901317. After 1 week of incubation, C26:0 levels in ALD fibroblasts were reduced by 50% ($P < 0.0001$), and after 2 and 3 weeks of incubation, the endogenous C26:0 levels were reduced to the levels observed in untreated control fibroblasts ($P < 0.0001$; Figure 5C).

To determine whether GW3965 and LXR623 have long-term effects on endogenous C26:0 levels similar to those of TO901317, ALD and control fibroblasts were cultured for 3 weeks with TO901317, GW3965, and LXR623, and the endogenous C26:0 levels were measured (Figure 5D). Compared with those in vehicle-treated ALD fibroblasts, C26:0 levels were significantly decreased after incubation with either TO901317, GW3965, or LXR 623 ($P < 0.0001$ for all). Also in control fibroblasts, the C26:0 levels were now significantly decreased after exposure to either of the 3 LXR agonists ($P < 0.0001$). Interestingly, there was no significant difference between the C26:0 levels of DMSO-treated control fibroblasts and the ALD fibroblasts cultured with TO901317, GW3965, or LXR623. The results of this experiment show that, with chronic treatment, LXR agonists reduced endogenous C26:0 levels in ALD fibroblasts to levels found in control fibroblasts.

Effect of TO901317 upon the composition of phospholipids. The VLCFAs that accumulate in the CNS of ALD patients are incorporated into many different lipid species, but the greatest excess has been reported in gangliosides (45) and phosphatidylcholine (PC) and cholesterol ester fractions (7, 46). VLCFA-enriched PC species are highly increased in intact myelin in ALD patients (46) and have been suggested as triggering the onset of disease. Indeed, injection of C24:0-LPC, but not C16:0-LPC, into WT mouse brain resulted in widespread microglial activation and apoptosis (18). To investigate whether exposure of ALD fibroblasts to LXR agonists affects not only total VLCFA levels, but also the composition of phospholipids, we performed lipidomic analysis. For this, 8 control and 8 ALD fibroblast cell lines were cultured with DMSO and 4 ALD fibroblast cell lines were cultured with 5 μM TO901317 for 3 weeks. We identified 1061 distinct lipid species. Comparison of the lipid profiles of control and ALD cells revealed an overall increase in PC species containing 2 fatty acids with a total number of more than 44 carbon atoms, which indicates an enrichment in VLCFA (Figure 6A).

Next, we investigated whether the correction in total VLCFA levels was also reflected in the ALD phospholipid profile. To this end, we compared control and ALD fibroblasts with ALD fibroblasts treated with TO901317 for 3 weeks. The heatmap (Figure 6B) shows the 50 lipid species that were most increased in ALD cells in comparison with control fibroblasts and the effect of TO901317 treatment on these lipid species. Treatment of ALD fibroblasts with TO901317 resulted in a complete correction in the majority of phospholipids. This is exemplified by the complete correction of C26:0-LPC (Figure 6C), which is the newborn screening biomarker for ALD (47–49).

Lipid-induced ER stress depends on the chain-length and saturation/desaturation status of fatty acids. Previously, we validated the use of VLCFA methyl esters to study VLCFA metabolism in whole cells and showed that the lipid-induced ER stress response in ALD fibroblasts is chain-length dependent, with the strongest effect with meC26:0 (23). To compare the toxicity of monounsaturated fatty acids and saturated fatty acids, we cultured control and ALD fibroblasts with equimolar concentrations of saturated long-chain (meC16:0, meC18:0, and meC20:0) and very long–chain (meC22:0, meC24:0, and meC26:0) fatty acids and monounsaturated long-chain (meC16:1, meC18:1, and meC20:1) and very long–chain (meC22:1, meC24:1 and meC26:1) fatty acids. As a marker for lipid-induced ER stress, XBP1s protein levels were measured (50). As a positive control for ER stress, control and ALD fibroblasts were exposed to tunicamycin, an inhibitor of *N*-linked glycosylation and
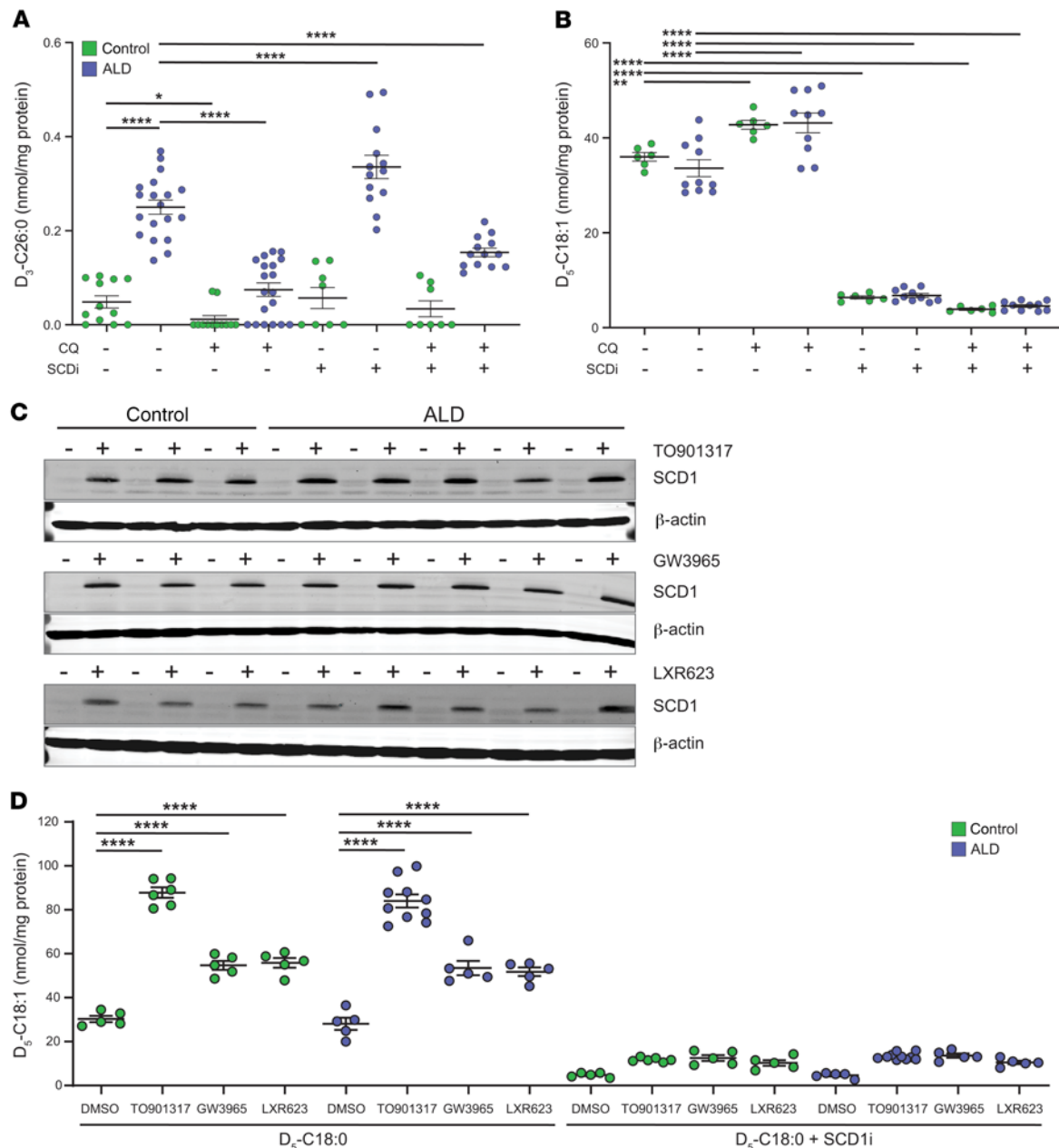
Figure 4. CQ and LXR agonists induce SCD1 protein and enzymatic activity. (**A**) CQ reduces de novo C26:0 synthesis in human primary fibroblasts. Control (n = 6) and ALD (n = 8) fibroblasts were cultured for 3 days with 100 μm D_3-C16:0 without and with CQ, SCD1 inhibitor (SCDi), or CQ + SCDi. De novo VLCFA synthesis was assessed by measuring the levels of D_3-C26:0 synthesized from D_3-C16:0. (**B**) Effect of CQ on SCD1 desaturase activity. Control (n = 3) and ALD (n = 5) were cultured for 24 hours with 100 μm D_5-C18:0 without and with CQ, SCDi, or CQ + SCDi. After 24 hours, the levels of D_5-C18:1 were determined. (**C**) Effect of LXR agonists on SCD1 protein induction. Control (n = 3) and ALD (n = 5) fibroblasts were cultured for 3 days with 0.1% (vol/vol) DMSO (–) or different LXR agonists (+): TO901317 (5 μM), GW3965 (1.5 μM), LXR623 (1.5 μM), and SCD1 protein levels were assessed by immunoblot analysis. β-Actin was used as a control for equal protein loading. (**D**) Effect of LXR agonists on SCD1 desaturase activity. Control (n = 5) and ALD (n = 5) fibroblasts were cultured for 24 hours with 100 μM D_5-C18:0 without and with SCD1i combined with 5 μM TO901317, 1.5 μM GW3965, or 1.5 μM LXR623. SCD1 desaturase activity was assessed by measuring the levels of D_5-C18:1 synthesized from D_5-C18:0. Final concentration DMSO in culture medium was less than 1% (vol/vol). Data are represented as mean ± SD. Statistical significance determined with 1-way ANOVA, followed by Tukey's multiple comparison test. *P < 0.05; **P < 0.01; ****P < 0.0001.

well known to induce ER stress. As expected, treatment of both control and ALD fibroblasts with tunicamycin caused increased XBP1s protein levels (Figure 7, A and B).

Exogenous exposure of control fibroblasts to either saturated or monounsaturated LCFA or VLCFA did not affect the expression of the XBP1s protein (Figure 7A). Exposure of ALD fibroblasts to sat-

urated and monounsaturated LCFAs (meC16–meC20), meC22:0, or monounsaturated VLCFAs did not result in increased XBP1s protein levels (Figure 7A). Only when ALD cells were incubated with the saturated VLCFA meC24:0 and meC26:0 were the levels of XBP1s protein markedly increased (Figure 7A). These results show that the lipid-induced ER stress response in ALD fibroblasts
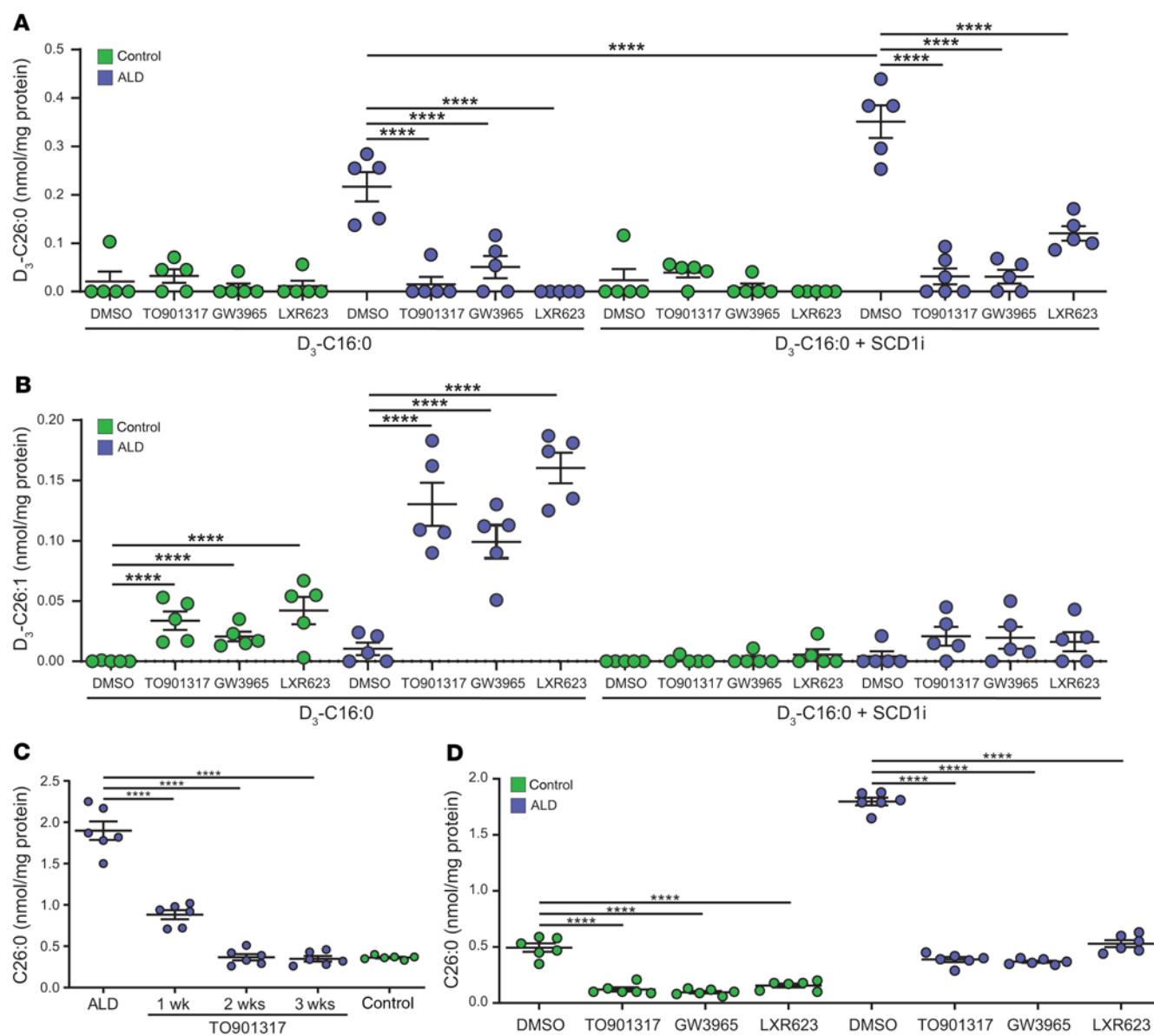
Figure 5. LXR agonists lower saturated VLCFA levels under acute and chronic exposure by shifting synthesis toward monounsaturated VLCFAs. (**A** and **B**) LXR agonists reduce de novo saturated VLCFA synthesis (**A**) and reroute toward monounsaturated VLCFA synthesis (**B**). Control ($n = 5$) and ALD ($n = 5$) fibroblasts were cultured for 3 days with 100 μM D_3-C16:0 without and with SCD1i combined with 5 μM TO901317, 1.5 μM GW3965, or 1.5 μM LXR623. De novo saturated VLCFA synthesis was assessed by measuring the levels of D_3-C26:0 synthesized from D_3-C16:0 (**A**). De novo monounsaturated VLCFA synthesis was assessed by measuring the levels of D_3-C26:1 synthesized from D_3-C16:0 (**B**). Inhibition of SCD1 enzymatic activity (SCDi) results in enhanced D_3-C26:0 synthesis and a complete block in D_3-C26:1 synthesis in ALD fibroblasts. (**C**) Chronic exposure to TO901317 normalizes endogenous C26:0 levels in ALD fibroblasts. ALD ($n = 6$) fibroblasts were cultured without and with 5 μM TO901317 up to 3 weeks. Total accumulated C26:0 levels were analyzed and compared with untreated control fibroblasts ($n = 5$). (**D**) Chronic exposure to LXR agonists normalizes endogenous C26:0 levels in control and ALD fibroblasts. Control ($n = 5$) and ALD ($n = 5$) fibroblasts were cultured for 3 weeks without and with 5 μM TO901317, 1.5 μM GW3965, or 1.5 μM LXR623, and the C26:0 levels were analyzed. Final concentration DMSO in culture medium was less than 1% (vol/vol). Data are represented as mean ± SD. Statistical significance determined with 1-way ANOVA, followed by Tukey's multiple comparison test. ****$P < 0.0001$.

is both chain-length dependent and specific for saturated VLCFA. Therefore, a shift in synthesis from the saturated VLCFAs toward monounsaturated VLCFAs may alleviate fatty acid toxicity in ALD.

TO901317 lowers C26:0 in Abcd1-deficient mouse CNS and adrenal gland. Abcd1-KO mice (*Abcd1$^{-/y}$*) develop a late axonopathy phenotype similar to that of human AMN patients. We investigated the effect of TO901317 supplementation upon VLCFA levels across different organs in the *Abcd1*-KO mouse.

Following 5 and 10 weeks of supplementation of mouse chow with TO901317, the levels of C26:0 were analyzed in mouse tissues and C26:0-lysoPC was analyzed in dried blood spots. The supplementation was with 100 mg/kg TO901317, based on the average weight of mice used in our experiments of approximately 33 g, each eating approximately 3.3 g chow/d. This corresponds to a daily intake of 330 μg TO901317, i.e., a daily dose of approximately 10 mg/kg body weight. In tissues, we observed a time-dependent
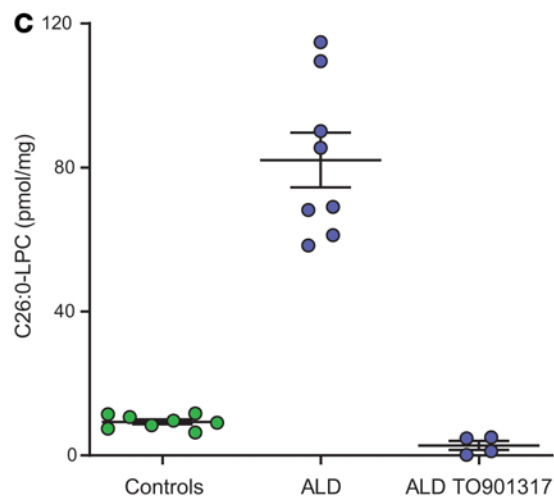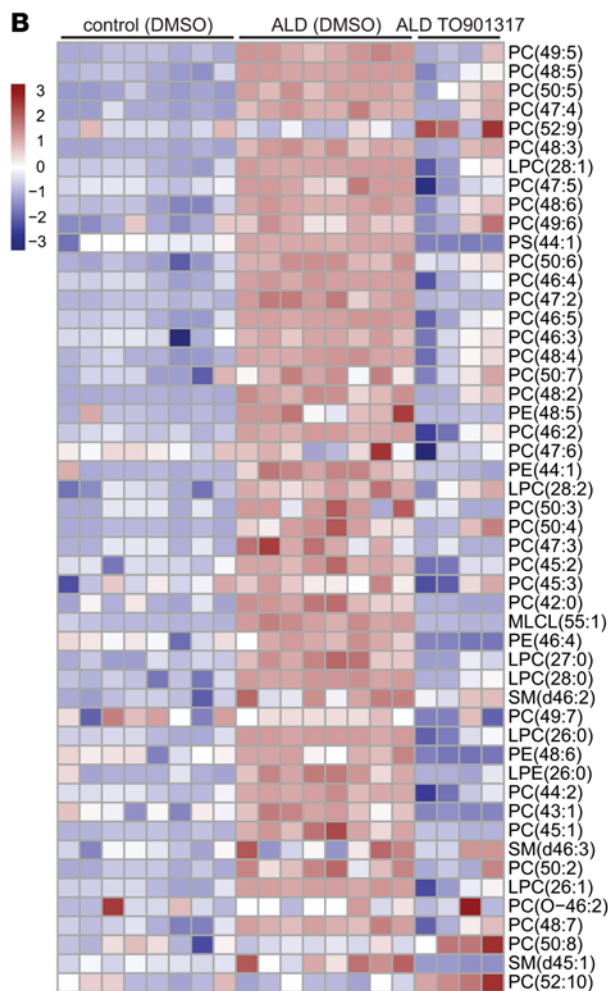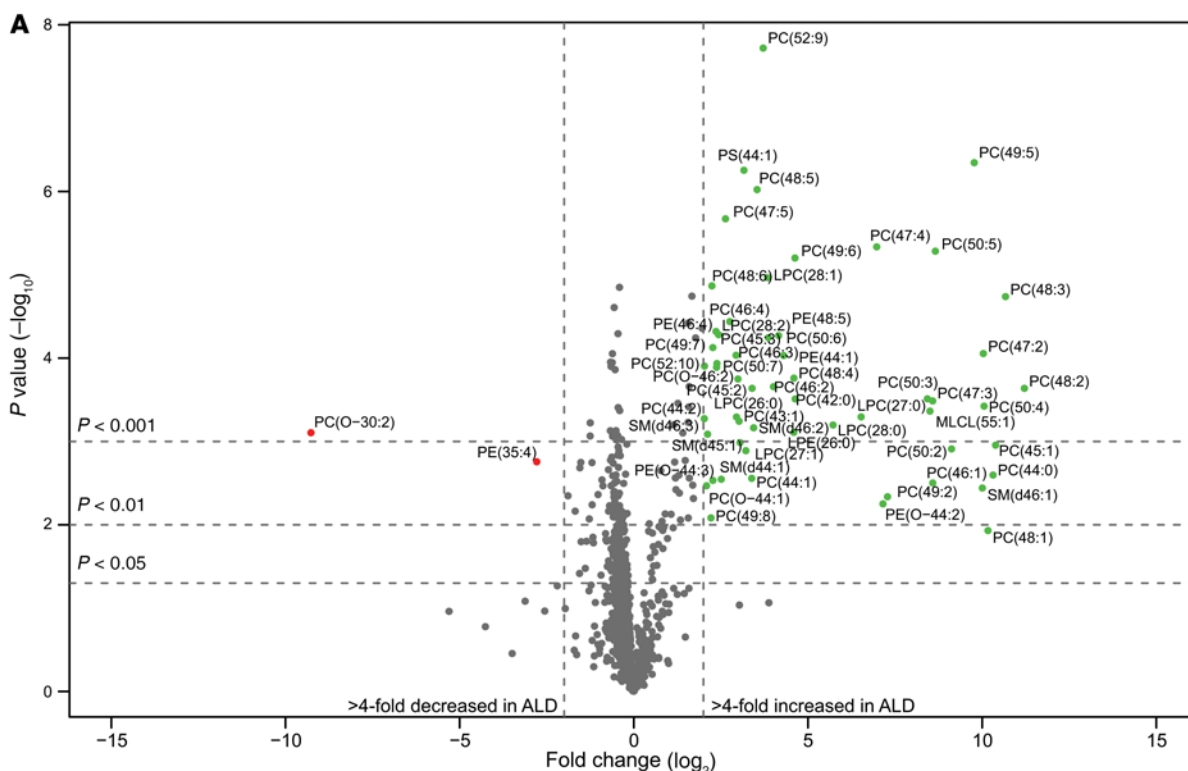
Figure 6. Lipid profiles in human ALD fibroblasts are corrected by LXR agonists. (**A**) Visualization of the comparison of the lipid profiles of control and ALD fibroblasts in a volcano plot. The *x* axis shows the $\log_2$ fold change in ALD cells and the *y* axis the significance of this change represented as $-\log_{10}$ (*P* value). Phospholipids are indicated as C(XX:Y), where XX indicates the total number of carbon atoms and Y the total number of double bonds in the fatty acyl chains. This analysis, without fragmentation, does not allow the specification of which fatty acid is located at the *sn*-1 or *sn*-2 position. Note an overall increase in PC species containing fatty acids with a total number of more than 44 carbon atoms, which indicates an enrichment in VLCFAs. Lipid species marked in red indicate a greater than 4-fold decrease and in green a less than 4-fold increase. (**B**) Heatmap showing the top 50 most changed lipid species based on the variable influence on projection (VIP) score extracted from the orthogonal projections to latent structures (OPLS). The left panel indicates samples from control fibroblasts (*n* = 8), the middle panel samples from ALD patient fibroblasts (*n* = 8), and the right panel samples from ALD fibroblasts treated with 5 μM TO901317 for 3 weeks (*n* = 4). Color in the heatmap reflects the logarithm of the relative lipid abundance, with red being higher and blue lower than the mean abundance value per lipid. (**C**) C26:0-LPC levels in control (*n* = 8), ALD (*n* = 8), and ALD fibroblasts after treatment with 5 μM TO901317 for 3 weeks (*n* = 4). Data are represented as mean ± SD.

decrease in C26:0 levels (Figure 8A). After 5 weeks, C26:0 levels in brain, spinal cord, and adrenal glands were 14%, 20% and 26% lower, respectively. After 10 weeks, C26:0 levels in brain, spinal cord, and adrenal glands were 19%, 20%, and 55% lower, respectively. C26:0-lysoPC levels in dried blood spots were reduced by 31% and 22% after 5 and 10 weeks, respectively (Figure 8B). Mice at the age of treatment (8 months at endpoint) did not display any overt neurological symptoms or other physical differences. No effects on body weight were seen in the treatment groups, and the compound was well tolerated in WT and *Abcd1*$^{-/y}$ mice, with modest weight loss after 10 weeks (Figure 8C). However, analysis of liver histology in both WT and mutants showed steatosis, cell ballooning, and active inflammation, all indicative of adverse effects from TO901317 (Supplemental Figure 3).

Our results of C26:0 lowering suggest that TO901317 was well absorbed and penetrated into compartments relevant to ALD and AMN. Indeed, analysis of TO901317 levels in brain and spinal cord revealed the presence of TO901317, albeit at lower (pmol) concentrations than those used in cell line experiments (Figure 8D).

Discussion

The accumulation of saturated VLCFA in peroxisomal disorders has vexed the field since their discovery in 1976 (7). Free fatty acids in the form of VLCFAs are more than 20 carbons in chain length, are not easily separated from membranes, and are thereby thought to disrupt membrane structure and cause ER stress (23, 28, 51). Attempts at lowering saturated VLCFAs have used a combination of dietary erucic and oleic acid, thereby adding to the pool of fatty acids and leading to an excess in monounsaturated fatty acids (41). Previously in peroxisomal disorders, the use of enzymatic induction to reroute saturated to monounsaturated VLCFAs, thereby keeping the overall pool of fatty acids constant, has not been attempted.

In this work, we demonstrate that a metabolic rerouting (Figure 9) reduces toxicity of VLCFAs to human cells in vitro and lowers saturated VLCFA amounts in *Abcd1*-deficient mice. This metabolic rerouting is mediated by SCD1, which we show is induced by CQ, identified from a compound screen in *abcd1* mutant zebrafish. CQ

normalized the abnormal motor phenotype in ALD zebrafish, and loss of *scd* phenocopied the *abcd1* mutant. In human fibroblasts, SCD1 activation increases the ratio of monounsaturated to saturated VLCFA; our work and that of others shows that exposure of saturated VLCFA to ALD cells causes oxidative stress, mitochondrial dysfunction, and an increase in the ER stress response (23, 25, 27, 28, 52). Using LXR agonists to preferentially target SCD1, we found that LXR agonists lower saturated VLCFA levels under acute and chronic exposure by a shift toward monounsaturated forms.

Our data consolidate findings regarding saturation status and ALD pathophysiology. Monounsaturated VLCFAs do not induce an ER stress response (23) and can in fact rescue ER stress caused by high levels of saturated fatty acids (24). We show that increased levels of XBP1s protein, a marker for ER stress, were only detected in ALD fibroblasts after incubation with the saturated, but not monounsaturated, VLCFAs.

Our findings highlight that SCD1 may be central to modulating VLCFA saturation status and hence a target for therapeutics. VLCFAs are synthesized de novo from saturated LCFAs, thereby generating intrinsically toxic saturated VLCFAs (20). SCD1 catalyzes the rate-limiting step in the conversion to monounsaturated fatty acids (29) by introduction of a *cis* double bond at the Δ-9 position (Figure 9). Based on prior work showing that LXR agonists increase SCD1 levels (44), we show that incubation of fibroblasts from ALD patients with LXR agonists (including TO901317, GW3965, and LXR623; refs. 53, 54) increased SCD1 protein levels and enzymatic activity. The addition of a SCD1 inhibitor (55) completely blocked the synthesis of monounsaturated fatty acids.

Further, we found that an increase in SCD1 activity resulted in a shift in the de novo fatty acids synthesis from saturated toward the monounsaturated VLCFAs. In the absence of LXR agonists, saturated VLCFA levels in ALD cells are elevated 10-fold (41). In the presence of LXR agonists, we found that saturated VLCFA levels in ALD cells were reduced to levels of control fibroblasts. Concurrently, the de novo synthesis of monounsaturated VLC-FAs was markedly increased in ALD fibroblasts after incubation with LXR agonists. This dual mechanism of rerouting (increased conversion to monounsaturated and increased monounsaturated synthesis) suggests a feedback pathway regulating VLCFA production and saturation status.

This is the first study, to our knowledge, that identifies compounds able to cause a complete normalization of saturated VLC-FA levels in ALD fibroblasts. Earlier studies reported reduced, but not normalized, endogenous C26:0 levels, including, for example, bezafibrate (30% reduction, ref. 21), 4-phenylbutyrate (47% reduction, ref. 56), and oleic acid (30% reduction, ref. 57). Given our successful reduction in fibroblasts, it is somewhat disappointing that we did not find the same reduction in vivo in *Abcd1*$^{-/y}$ mice. However, it seems likely that this only partial reduction is related to the duration of dosing (10 weeks), bioavailability of the compound and achievable drug concentrations, and potentially to the efficacy of the LXR agonists we used. We found, for example, that levels of the LXR agonist TO901317 were approximately 2 to 3 times lower in the brain and spinal cord than in the liver. Also, even with this dosage, there was substantial liver toxicity.

An important additional note is that even with AAV9 -or HSCT-mediated gene therapy, there was only partial reduction of
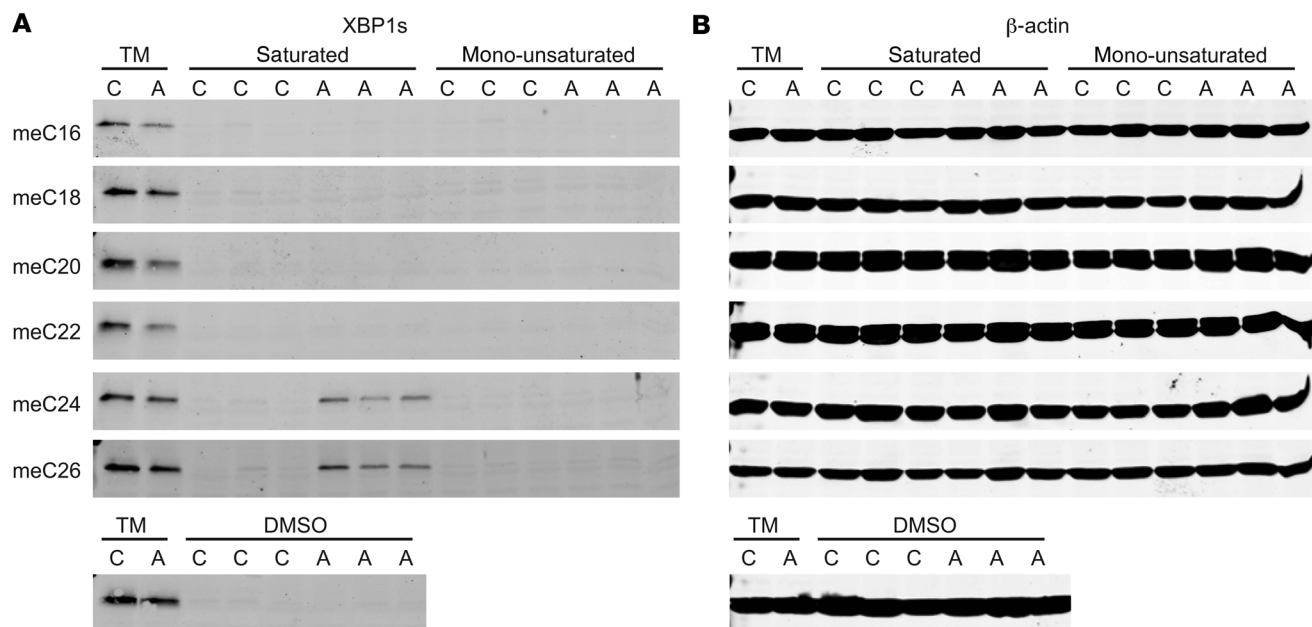
Figure 7. ER stress caused by saturated VLCFAs. (**A**) Immunoblot analysis of XBP1s protein after incubation with saturated and monounsaturated fatty acids. Control (C) and ALD (A) fibroblasts were incubated for 1 day with 10 μg/mL tunicamycin (TM) or for 4 days with 60 μM of long-chain (meC16–meC20) and very long–chain (meC22 - meC26) fatty acids. The effect of treatment on XBP1s protein levels was determined in control (*n* = 3) and ALD (*n* = 3) fibroblasts. (**B**) β-actin was used as control for equal amount of protein loading.

VLCFA levels (58, 59). Given that overreduction of C26:0 levels can have adverse side effects (see paragraph immediately below), perhaps achieving sufficient but not excessive reduction will be important. As new agents are identified that have higher efficacy and lower toxicity, it will be important to compare fibroblast versus whole animal C26:0 lowering as well as phenotypic effects.

It is important to note that treatment of ALD cells with LXR agonists did not reduce C26:0 levels below that found in untreated control cells. Saturated VLCFAs are essential because they are part of complex lipids in cell membranes and myelin. For example, the epidermal barrier of the skin consists of approximately 50% ceramides, 25% cholesterol, and 15% long- and very long–chain fatty acids (60), and LXR agonists and antagonists can modulate lipid composition and affect skin organization and thickness (61). There is a potential that reduction in saturated VLCFAs to subnormal levels may cause deleterious effects. For example, Elovl1-KO mice, in which synthesis of VLCFA-containing lipids is disrupted, died shortly after birth due to epidermal barrier defects (62). Furthermore, a phase 1 clinical trial to evaluate safety and tolerability of LXR623 in healthy subjects reported CNS-related adverse events and neurologic- or psychiatric-related adverse events (63). However, the subjects in this trial did not suffer from a peroxisomal β-oxidation disorder and therefore did not have increased VLCFA levels. Therefore, we cannot rule out that further reduction of low levels of saturated VLCFAs during LXR623 treatment might have contributed to some of the adverse effects reported in this study.

Finally, our study revealed data about the large differences in the phospholipid profile between control and ALD fibroblasts that were partially normalized by LXR agonist treatment. Comparison of the lipid profiles of control and ALD cells revealed an overall increase in PC species containing fatty acids with a total

number of more than 44 carbon atoms, which indicates an enrichment in VLCFAs. These PC species are potential new biomarkers for ALD, but will require further confirmation. Upon treatment with TO901317, almost all phospholipid species elevated in ALD fibroblasts were reduced to levels seen in control fibroblasts. Interestingly, the levels of C26:0-LPC, the marker that is used in newborn screening to detect ALD (47, 64), are completely normalized in ALD fibroblasts upon treatment with TO901317. Since ALD is a peroxisomal defect, it will also be interesting in future work to look at the response of plasmalogen levels to CQ or other inducers of SCD1 expression, particularly as plasmalogen deficiency has been associated with cerebral ALD (65).

The concept of increasing SCD1 activity or expression, and thus the use of LXR agonists, has implications for treatment in ALD. One of the reasons is that saturated VLCFAs induce lipoapoptosis in ALD fibroblasts (23). Therefore, increased levels of SCD1 protein might be protective against lipoapoptosis in ALD. Indeed, it has been shown that overexpression of SCD1 in renal proximal tubular epithelial cells protects against lipoapoptosis induced by palmitic acid (C16:0) (66). Another intriguing possibility is that LXR agonists can reduce or modulate inflammation and thus might have an additional role in ALD to counter the inflammation observed in cerebral ALD. For example, TO901317 protects against CNS inflammation in injury models (67, 68). However, in other settings, LXR agonists appear to induce a proinflammatory state (69–71). Finally, LXR agonists also differentially affect expression of myelin genes, such as PLP1 and MBP, which could affect the potential for remyelination or protection against myelin loss (72).

An interesting question our work did not address was that of whether prolonged treatment would reduce axonal degeneration. For example, we currently do not know whether treatment of the
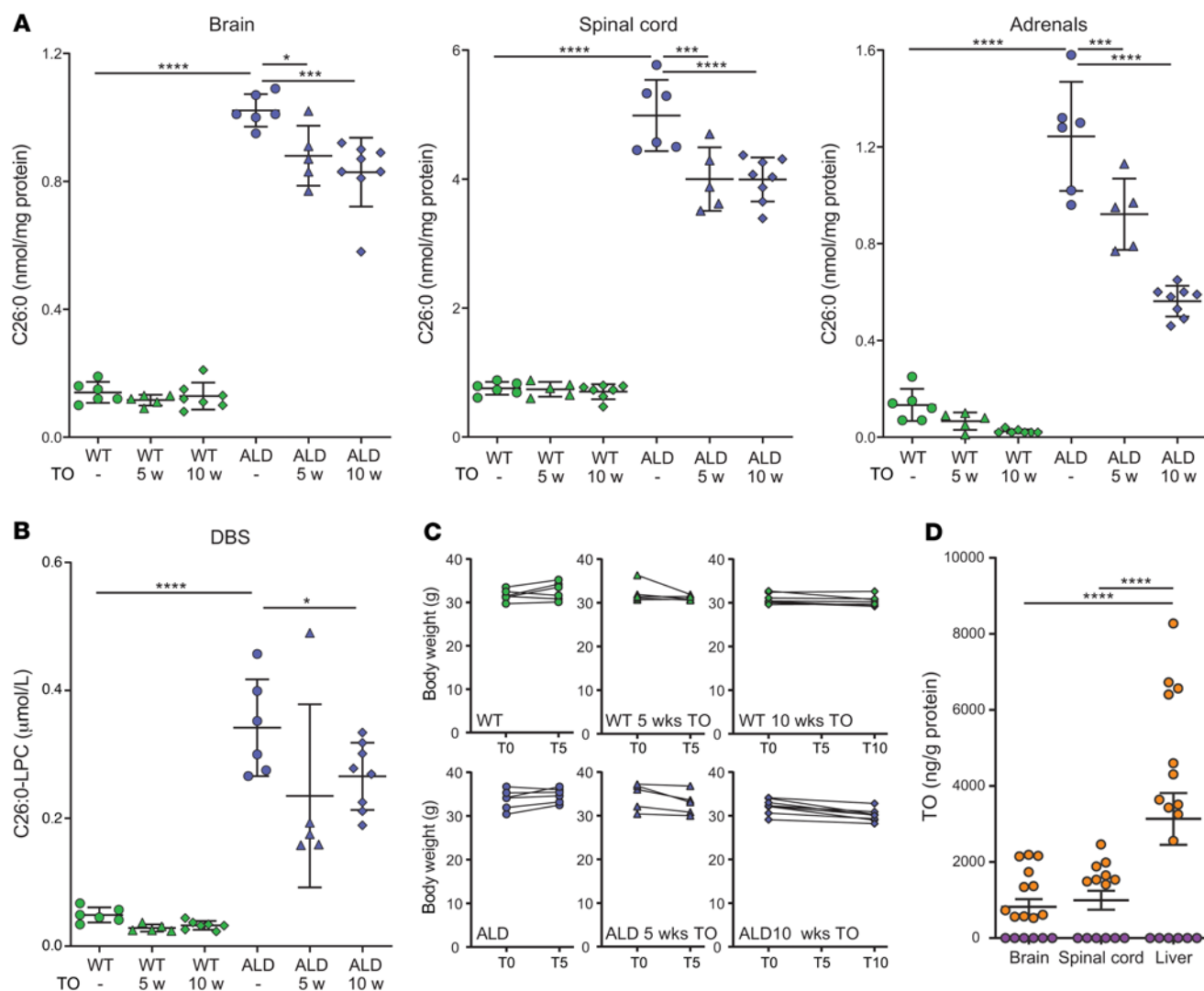
Figure 8. Pharmacologic induction of SCD1 via TO901317 lowers C26:0 in the CNS and adrenal gland of *Abcd1*-deficient mice. (**A–C**) WT (green) and *Abcd1⁻/y* mice (ALD in blue) received standard mouse chow (n = 6/group), whereas the treatment arms received chow supplemented with 100 mg/kg TO901317 (TO) for either 5 (n = 5/group) or 10 (n = 7/group) weeks (WT 5 w and 10 w versus ALD 5 w and 10 w). The effect of treatment on C26:0 levels was evaluated in brain, spinal cord, and adrenal glands (**A**) and on C26:0-LPC in dried blood spots (DBS) (**B**). Body weights were recorded weekly and did not show toxicity in the TO treatment groups (**C**). Values in **A** and **B** are represented as mean ± SD. Statistical significance was determined with 1-way ANOVA, followed by Tukey's multiple comparison test. $*P < 0.05$; $***P < 0.001$; $****P < 0.0001$. (**D**). TO levels were determined in untreated (purple) and TO (10 w) treated mice (orange).

Abcd1⁻/y mice with the LXR agonist TO901317 for longer than 8 months would prevent the late-onset axonal degeneration similar to that seen in AMN patients (30). A longer readout of LXR effects is important and will require an improved compound — either an LXR agonist–related compound, or a different compound that induces *SCD1*, with lower toxicities.

Our identification that a metabolic rerouting of fatty acids and their saturation status modulates ALD pathophysiology also suggests treatment considerations for other conditions. While SCD1-mediated rerouting toward monounsaturated forms is protective for ALD models, saturated VLCFA appear to confer protective effects for type 2 diabetes, heart failure, and cancer stem cells (73–75). Understanding how saturation status of fatty acids affects these diverse disease processes, ranging from ALD neurodegeneration to cancer stem cell maintenance, is an important next step.

Although promising, pursuit of CQ or of LXR agonists as potential treatments for AMN has notable limitations and was not a primary purpose of this work. Treatment for AMN may need to be initiated during adolescence or even earlier to be of maximal benefit, and thus any exposure to a compound will be for multiple decades. CQ or hydroxychloroquine, a metabolite of CQ, has a narrow therapeutic window, causes retinal toxicity in as many as 20% of patients (76), and has been associated with serious cardiac complications, including arrhythmias, cardiomyopathy, and death (77). Currently available LXR agonists have significant side effects, including in particular hepatic steatosis and hypertriglyceridemia (78–80), and have not been approved for clinical use (81).

Additional studies into the mechanism or mechanisms of action of CQ and LXR agonists in ALD and fatty acid saturation status and identification of compounds with lower toxicity
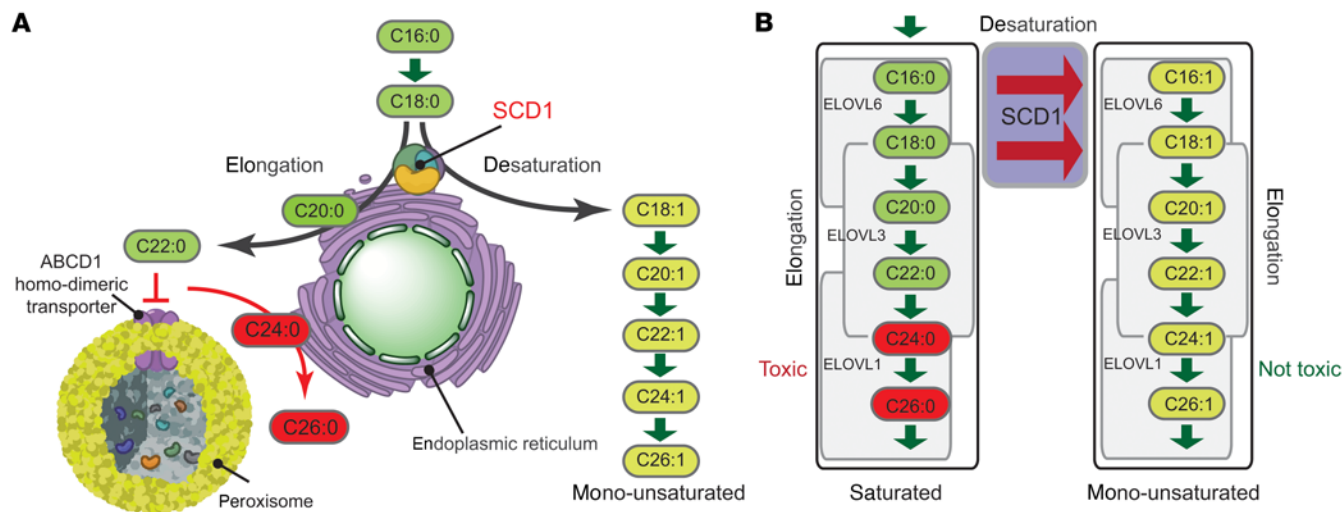
Figure 9. Overview of metabolic rerouting in ALD. (A) ALD is caused by mutations in the *ABCD1* gene that produces the ABCD1 protein, a transporter of VLCFAs from the cytosol into the peroxisomes. A deficiency in ABCD1 blocks this transport, which results in impaired degradation and a subsequent build-up of VLCFAs in cells, tissues, and organs. **(B)** VLCFAs are synthesized through LCFA elongation largely controlled by ELOVL1. Activation of SCD1 causes a shift from the saturated toward the monounsaturated fatty acids.

and more selectivity are needed prior to clinical trials. An option to further characterize these questions is through RNA-Seq of CQ-treated animals, which would provide information on the relative increase in *SCD1* expression needed and could also provide further insights on mechanism of action.

In summary, we report the use of an in vivo phenotype-based compound screen to identify SCD1 as a key modulator of ALD pathophysiology. We show that SCD1 induction reduced ALD-related motor impairments in zebrafish, reduced VLCFA levels in ALD fibroblasts, and increased the ratio of monounsaturated to saturated VLCFAs. LXR agonists, acting specifically to induce SCD1, reduced VLCFA accumulation in *Abcd1*-deficient mice and partially normalized phospholipid profiles. We suggest that targeting of SCD1, or the metabolic pathway or pathways integral to the saturation status of VLCFAs, is a promising avenue for treatment of the chronic myelopathy of ALD. Our results show a role for metabolic rerouting in ALD pathophysiology and offer insight into the use of biochemical pathway modulation to improve neurometabolic diseases.

Methods

Zebrafish husbandry and lines

Adult fish were bred according to standard methods. Embryos were raised at 28.5°C in E3 embryo medium and staged by time and morphology. Transgenic fish lines and alleles used in this paper were the following: Tg(*olig2:dsRed*), *abcd1*[sa509], and *abcd1*[zc92], as described previously (32).

Zebrafish drug screening

For the primary drug screen, single zebrafish larvae aged 3 days after fertilization from *abcd1*[sa509/sa509] parents were plated in 96-well square-bottom plates in E3 embryo medium. Groups of 12 larvae were incubated with 4 compounds, 10 μM each in DMSO 0.1%, from the 2560 compounds of the Microsource Spectrum Collection (MicroSource Discovery Systems Inc.) from 4 to 7 days after fertilization.

Similarly, for the secondary screen, groups of 30 larvae from *abcd1*[WT/WT] or *abcd1*[sa509/sa509] parents were incubated with the selected drugs (MilliporeSigma), 10 μM each in DMSO 0.1% from 4 to 7 days after fertilization. For further validation, groups of 100 larvae from *abcd1*[sa509/sa509] or *abcd1*[zc92/zc92] were incubated with CQ diphosphate salt (MilliporeSigma), 1, 2.5, or 10 μM directly solubilized in E3 medium; prednisolone (Sigma), 1, 2.5, or 10 μM, DMSO 0.1% in E3 medium; or bafilomycin A1 (Invitrogen) 10, 100, or 1000 nM, DMSO 0.1% in E3 medium.

Zebrafish behavior analysis

After incubating with the drugs for 24, 48, or 72 hours, single larvae's motor behaviors were recorded using the Noldus DanioVision Observation Chamber and analyzed with EthoVision XT software. Animals were allowed to adapt in the light for 10 minutes, and then recording was performed for 5 minutes (1 minute light and 4 minutes dark). The distance (in mm) and time spent moving (in seconds) by larvae during 5 minutes were analyzed, and variations between treatments for each variable were displayed as a *z* score calculated for groups of larvae of the same age and genotype.

Zebrafish scd and scdb CRISPR

CRISPR mutagenesis targeting the *Danio rerio scd* and *scdb* genes (Ensembl Zv10: ENSDARG00000033662 and ENSDARG00000030265) was performed designing sgRNA target sites by looking for sequences corresponding to N18GG on the sense or antisense strand of the DNA using the CRISPR design program (http://crispr.mit.edu). Off-target effects were checked through the use of NIH BLAST tool applied to the zebrafish genome (zv10). Off-target sequences that had significant matches of the final 23 nt of the target and NGG PAM sequence were discarded. sgRNAs targeting exon 1 of *scd* and *scdb* genes were transcribed using DraI-digested gRNA expression vectors as templates and the HiScribe T7 RNA Synthesis Kit (New England BioLabs), followed by RNA purification with Micro Bio-Spin 6 columns (Bio-Rad). Two sgRNAs targeting exon 1 of *scd* (scd sg1) 5′-GCCCCAGCTGGAGGCAATGG-3′ and (scd

sg2) 5′-CCCTTATATAAAGAGAAACC-3′ (scdb sg1), or exon 1 of *scdb* 5′-CGATGTGACGACGACGACAG-3′ and (scdb sg2) 5′-CTCTGTC-GTCGTCGTCACAT-3′ were simultaneously injected. Embryos from the 1- to 4-cell stage were microinjected with 500 pl of 200 ng/l sgR-NA and 200 ng/l Cas9 mRNA. Lethality up to 6 dpf was controlled in each group until motor behavior of larvae was recorded. Disruption of coding sequence in *scd* and *scdb* genes was confirmed using HRMA.

Zebrafish genotyping

DNA was extracted from whole embryos (24 hpf–72 hpf) or tail or fin clips into 50 mM NaOH and incubated at 95°C for 20 minutes, followed by neutralization with 1 M Tris pH 8.0 (1:10 by volume), as previously described (82). PCR was performed using the LightScanner Master Mix System (BioFire) in 10 μl reactions, as previously described (82). Thermal melt profiles were collected on a LightScanner (Idaho Technology) (65–98°C, hold 62°C) and analyzed with LightScanner Software. For *scd* and *scdb* alleles with mutations in exon 1, we used the following primers and conditions: (scd forward primer) 5′-CATCATCATGCCTGATTCTGATGTG-3′ and (scd reverse primer) 5′-CAGAATGACATTTCGCCACACTA-3′; (scdb forward primer) 5′-GAGGCAGTACACGAGCACAG-3′ and (scdb reverse primer) 5′-CTCCATACGATTTGTACCGGAGGAC-3′; 95°C for 2 minutes, followed by 29 cycles of 95°C for 30 seconds, and 60°C for 30 seconds, followed by a final denaturation and annealing step of 95°C for 30 seconds and 25°C for 30 seconds. For *abcd1*^{sa509} and *abcd1*^{Zc92} alleles, we used the following primers and conditions: (sa509 forward primer) 5′-TTACTCACCGTCCTTCTCTC-3′, (sa509 reverse primer) 5′-TCATACGATTCAAAACCCAC-3′ (zc92 forward primer) 5′-GTG-GCTCATCTGTATTCAAACCT-3′, and (zc92 reverse primer)5′-CAG-CCGTTTTAATGAGCGTGTA-3′; 95°C for 2 minutes, followed by 29 cycles of 95°C for 30 seconds, and 68.1°C for 30 seconds, followed by a final denaturation and annealing step of 95°C for 30 seconds and 25°C for 30 seconds. All PCR assays were run in an optically transparent plate with 25 l mineral oil overlay. We then performed HRMA to differentiate the melt curves from their corresponding controls.

Zebrafish microscopy and image analysis

Transgenic *olig2:dsRed/abcd1*^{sa509} larvae or their WT siblings were treated with phenylthiourea from 24 hpf and received CQ (10 μM) from 3 to 5 dpf. Larvae were euthanized by submersion in ice water followed by fixation in paraformaldehyde (PFA) overnight at 4°C. Larvae were dehydrated in methanol at –20°C for 2 hours and then rehydrated in PBS, 0.1% Tween-20 (PBST). Tissue permeabilization was facilitated using proteinase K (10 μg/ml) for 1 hour at 28°C followed by a postfixation step, 15 minutes in PFA. Larvae were incubated in PBST + 1% DMSO + 2% BSA + 5% normal goat serum (NGS) for 2 hours and then, in the presence of the Living Colors DsRed Rabbit Polyclonal Antibody (Takara), 1:400 overnight at 4°C. Next, larvae were washed thoroughly in PBST + 1% DMSO + 1% NGS and incubated in the presence of goat anti-rabbit IgG (H+L), Alexa Fluor 555 secondary antibody (Invitrogen) overnight at 4°C. Larvae were washed thoroughly and finally transferred in mounting media containing 80% glycerol/20% PBS. At this stage, the tail was clipped for genotyping and the samples were mounted on a glass slide with a #0 coverslip for imaging under a confocal microscope. Using ImageJ (NIH), confocal stacks were generated using a max intensity projection and cell counts were performed manually in the delimited area.

Zebrafish RNA extraction and qRT-PCR

RNA from 6 larvae, aged 7 dpf, was extracted for 5 to 6 independent samples. Each sample was suspended in 250 μl TRIzol Reagent (Invitrogen) and homogenized using pellet pestles until no tissue remained visible. The homogenized samples were briefly incubated for 2 minutes at room temperature and gently mixed after the addition of 50 μl of chloroform, followed by centrifugation for 15 minutes at 12,000g at 4°C. The aqueous phase was moved to a new tube, and an equal volume of 70% ethanol was added. RNA were then isolated using the Ambion PureLink RNA Mini Kit (Thermo Fisher Scientific). First-strand cDNA was made from 1 μg total RNA using SuperScript IV VILO Master Mix (Invitrogen) after removal of genomic DNA using the ezDNase (Thermo Fisher Scientific). All quantitative reverse-transcriptase PCR (qRT-PCR) reactions were performed using SYBR Green PCR Master Mix (Invitrogen); primer sequences and conditions are in the Supplemental Methods.

Cell culture

Human primary skin fibroblast cell lines were obtained from ALD patients through the Neurology Outpatient Clinic of Amsterdam UMC. The diagnosis of ALD was confirmed via VLCFA and *ABCD1* mutation analysis (p.Met1Val; p.Asp194His; p.Glu278*; p.Ser284*; p.Arg389His; p.Gln472Argfs*83; p.Pro480Thr; p.Leu654Pro). Control fibroblasts were obtained from anonymous male volunteers. Cells were cultured as described (23). In each experiment, the final concentration of DMSO in culture medium was equal (≤1% vol/vol) in all conditions.

Mice

The study included adult male littermates, carrying either an *Abcd1*$^{+/y}$ (WT) or *Abcd1*$^{-/y}$ (*Abcd1*^{tm1Kan}/J, KO) allele (83) that had been backcrossed for at least 20 generations onto the C57BL/6J strain. Mice were housed at the animal facility of the Center for Brain Research, Medical University of Vienna, in an environmentally controlled room on a 12-hour light/12-hour dark cycle and with ad libitum access to water and chow. The mice were maintained on standard rodent chow (R/M-H, Ssniff) until the start of the study. The average daily consumption was 3.3 g of chow for mice with a body weight of around 33 g.

At the age of 25 to 28 weeks, WT ($n = 18$) and *Abcd1*$^{-/y}$ ($n = 19$) mice were randomly distributed into 6 groups (group 1, 6 WT; group 2, 5 WT; group 3, 7 WT; group 4, 6 *Abcd1*$^{-/y}$; group 5, 5 *Abcd1*$^{-/y}$; and group 6, 8 *Abcd1*$^{-/y}$ mice). Groups 1 and 4 received standard chow (R/M-H). Groups 2 and 4 received R/M+H chow supplemented with 100 mg/kg TO901317 (Cayman Chemical, pressed into pellets by Ssniff) for 5 weeks, and groups 3 and 6 received the TO901317-supplemented chow for 10 weeks. Mice in the study were observed daily and monitored more closely 3 times/week;body weight was recorded weekly. None of the animals showed any signs of distress or illness or died during the study. For tissue collection, the mice were killed by carbon dioxide inhalation at a rate sufficient to induce rapid anesthesia, with death occurring within 2.5 minutes.

Liver histopathology

For histopathological assessment of the liver following TO treatment, cross sections (1 to 1.5 mm thick) of the left liver lobe from each mouse were dissected at the treatment endpoint, immersion fixed, embedded in paraffin, and stained with H&E and PAS. Full details and scoring (Bedossa et al.; ref. 84) are provided in the Supplemental Methods.

Chemicals and antibodies

Full lists and details are provided in the Supplemental Methods. Methyl esters of C26:0 (meC26:0) and C26:1 (meC26:1) were prepared as described previously (23).

Analysis of TO901317

Sample preparation was performed essentially as described, with minor modifications; see Supplemental Methods for full details (73, 85).

VLCFA analysis

Desaturation assay and de novo fatty acid synthesis. To inhibit SCD1, cells were preincubated overnight with 100 nM SCD1 inhibitor (BioVision 1716). The next day, the culture medium was replaced by culture medium with 100 μM D_5-C18:0 or 100 μM D_3-C16:0 combined with the different compounds, as indicated in the figure legends. After 24 hours (D_5-C18:0, desaturation assay) or 72 hours (D_3-C16:0, de novo synthesis assay), cells were harvested by trypsinization and rinsed twice with PBS; pellets were homogenized in deionized water via sonication on ice with a needle (12 seconds at 7-8 watts). Pierce bicinchoninic acid (BCA) protein assay was used to determine the protein concentration; 150 μg protein was used for the desaturation assay, as described previously (55, 86), or the de novo VLCFA synthesis assay, as described previously (87, 88). VLCFA levels were analyzed by electrospray ionization mass spectrometry, as described previously (42).

Endogenous fatty acid levels. Cells were incubated with compounds or vehicle DMSO. Concentrations and incubation times are indicated in the figure legends. Culture medium and compounds were refreshed every 5 days. After incubation, the cells were harvested by trypsinization. For fatty acid analysis, 150 μg protein was used as described previously (42).

Lipidomics

Cells were incubated with 5 μM TO901317 or vehicle (DMSO) for 3 weeks, after which the cells were harvested by trypsinization. Lipidomics was performed as described (16).

Immunoblotting

See Supplemental Methods for full details. For XBP1s, fibroblasts were incubated with fatty acids as described previously (23). For SCD1, control and ALD fibroblasts were seeded at approximately 40% confluence. All incubations were performed at room temperature. Fluorescently labeled proteins were detected by LI-COR Odyssey.

Statistics

All statistical analyses were performed using GraphPad Prism, version 6.0. Statistical comparisons were made using 1-way ANOVA followed by Bonferroni's, Dunnett's, or Tukey's multiple comparisons test or 2-way ANOVA followed by Bonferroni's multiple comparisons test, as indicated in figure legends. $P < 0.05$ was used as the criterion for statistical significance. Bioinformatics and statistical analysis of the lipidomics data was performed as described previously (16).

Study approval

Human primary skin fibroblast cell lines were obtained from ALD patients through the Neurology Outpatient Clinic of Amsterdam UMC. At the time of writing, all ALD patients are participating in a prospective natural history study with annual follow-up (IRB: METC 2014_347). Material from these patients was obtained from the Peroxisomal Biobank from the Amsterdam UMC (IRB: METC 2015_066). Written, informed consent was obtained from each patient and men in control group.

WT and *Abcd1$^{-/y}$* mice were bred and housed at the animal facility of the Center for Brain Research, Medical University of Vienna, and received humane care and handling in compliance with institutional and national (Austrian) regulations (BGBl. II Nr. 522/2012) and European Union Directive 2010/63/EU. Procedures for the mice were reviewed and approved by the local Animal Care and Use Committee of the Medical University of Vienna and by the Austrian Federal Ministry of Education for Science and Research (BMBWF-66.009/0174-V/3b/2019).

Zebrafish work was performed in strict accordance with guidelines from the University of Utah IACUC, regulated under federal law (the Animal Welfare Act and Public Health Services Regulation Act) by the US Department of Agriculture (USDA) and the Office of Laboratory Animal Welfare at the NIH, and accredited by the Association for Assessment and Accreditation of Laboratory Care International (AAALAC).

Author contributions

MCVDB, RJAW, ME, FE, JLB, and SK designed the studies. QR, MCVDB, SFP, IMED, AD, BCF, TJS, LN, YRJJ, JYEL, and AD conducted experiments. QR, MCVDB, TJS, MVW, BCF, AD, YRJJ, and JYEL acquired data. MCVDB, SFP, FE, JB, JLB, and SK wrote the manuscript. All authors participated in analyzing data, reviewing the manuscript, and providing final critical approval. QR was designated as first listed coauthor on the basis of performing more of the experiments used in the manuscript.

Address correspondence to: Joshua L. Bonkowsky, Department of Pediatrics, 295 Chipeta Way, Salt Lake City, Utah 84108, USA. Phone: 801.213.3599; Email: joshua.bonkowsky@hsc.utah.edu. Or to: Stephan Kemp, Amsterdam UMC, Departments of Clinical Chemistry and Pediatrics, Room F0-212, Meibergdreef 9, 1105AZ Amsterdam, The Netherlands. Phone: 31.20.5660158; Email: s.kemp@amsterdamumc.nl.

1. Mosser J, et al. Putative X-linked adrenoleukodystrophy gene shares unexpected homology with ABC transporters. *Nature*. 1993;361(6414):726–730.
2. van Roermund CW, et al. The human peroxisomal ABC half transporter ALDP functions as a homodimer and accepts acyl-CoA esters. *FASEB J*. 2008;22(12):4201–4208.
3. Wiesinger C, et al. Impaired very-long-chain acyl-CoA β-oxidation in human X-linked adrenoleukodystrophy fibroblasts is a direct consequence of ABCD1 transporter dysfunction. *J Biol Chem*. 2013;288(26):19269–19279.
4. Singh I, et al. Adrenoleukodystrophy: impaired oxidation of very long chain fatty acids in white blood cells, cultured skin fibroblasts, and amniocytes. *Pediatr Res*. 1984;18(3):286–290.
5. Moser AB, et al. Plasma very long chain fatty acids

in 3,000 peroxisome disease patients and 29,000 controls. *Ann Neurol*. 1999;45(1):100–110.

6. Moser HW, et al. X-linked adrenoleukodystrophy. In: Scriver CR, et al, eds. *The Metabolic and Molecular Bases of Inherited Disease*. McGraw Hill; 2001:3257–3301

7. Igarashi M, et al. Fatty acid abnormality in adrenoleukodystrophy. *J Neurochem*. 1976;26(4):851–860.

8. van de Beek MC, et al. C26:0-Carnitine is a new biomarker for X-linked adrenoleukodystrophy in mice and man. *PLoS One*. 2016;11(4):e0154597.

9. Kemp S, et al. Adrenoleukodystrophy — Neuroendocrine pathogenesis and redefinition of natural history. *Nat Rev Endocrinol*. 2016;12(10):606–615.

10. Dubey P, et al. Adrenal insufficiency in asymptomatic adrenoleukodystrophy patients identified by very long-chain fatty acid screening. *J Pediatr*. 2005;146(4):528–532.

11. Huffnagel IC, et al. The natural history of adrenal insufficiency in X-linked adrenoleukodystrophy: an international collaboration. *J Clin Endocrinol Metab*. 2019;104(1):118–126.

12. Engelen M, et al. X-linked adrenoleukodystrophy (X-ALD): clinical presentation and guidelines for diagnosis, follow-up and management. *Orphanet J Rare Dis*. 2012;7(1):51.

13. Beckmann NB, et al. Quality of life among boys with adrenoleukodystrophy following hematopoietic stem cell transplant. *Child Neuropsychol*. 2018;24(7):986–998.

14. Miller WP, et al. Outcomes after allogeneic hematopoietic cell transplantation for childhood cerebral adrenoleukodystrophy: the largest single-institution cohort report. *Blood*. 2011;118(7):1971–1978.

15. Engelen M, et al. X-linked adrenoleukodystrophy in women: a cross-sectional cohort study. *Brain*. 2014;137(3):693–706.

16. Huffnagel IC, et al. Disease progression in women with X-linked adrenoleukodystrophy is slow. *Orphanet J Rare Dis*. 2019;14(1):30.

17. van Geel BM, et al. Hematopoietic cell transplantation does not prevent myelopathy in X-linked adrenoleukodystrophy: a retrospective study. *J Inherit Metab Dis*. 2015;38(2):359–361.

18. Eichler FS, et al. Is microglial apoptosis an early pathogenic change in cerebral X-linked adrenoleukodystrophy? *Ann Neurol*. 2008;63(6):729–742.

19. Hein S, et al. Toxic effects of X-linked adrenoleukodystrophy-associated, very long chain fatty acids on glial cells and neurons from rat hippocampus in culture. *Hum Mol Genet*. 2008;17(12):1750–1761.

20. Ofman R, et al. The role of ELOVL1 in very long-chain fatty acid homeostasis and X-linked adrenoleukodystrophy. *EMBO Mol Med*. 2010;2(3):90–97.

21. Engelen M, et al. Bezafibrate lowers very long-chain fatty acids in X-linked adrenoleukodystrophy fibroblasts by inhibiting fatty acid elongation. *J Inherit Metab Dis*. 2012;35(6):1137–1145.

22. Schackmann MJA, et al. Enzymatic characterization of ELOVL1, a key enzyme in very long-chain fatty acid synthesis. *Biochim Biophys Acta*. 2015;1851(2):231–237.

23. van de Beek MC, et al. Lipid-induced endoplasmic reticulum stress in X-linked adrenoleukodystrophy. *Biochim Biophys Acta*. 2017;1863(9):2255–2265.

24. Volmer R, et al. Membrane lipid saturation activates endoplasmic reticulum unfolded protein response transducers through their transmembrane domains. *Proc Natl Acad Sci U S A*. 2013;110(12):4628–4633.

25. Fourcade S, et al. Early oxidative damage underlying neurodegeneration in X-adrenoleukodystrophy. *Hum Mol Genet*. 2008;17(12):1762–1773.

26. Launay N, et al. Oxidative stress regulates the ubiquitin-proteasome system and immunoproteasome functioning in a mouse model of X-adrenoleukodystrophy. *Brain*. 2013;136(Pt 3):891–904.

27. Lopez-Erauskin J, et al. Impaired mitochondrial oxidative phosphorylation in the peroxisomal disease X-linked adrenoleukodystrophy. *Hum Mol Genet*. 2013;22(16):3296–3305.

28. Launay N, et al. Tauroursodeoxycholic bile acid arrests axonal degeneration by inhibiting the unfolded protein response in X-linked adrenoleukodystrophy. *Acta Neuropathol*. 2017;133(2):283–301.

29. Ntambi JM, Miyazaki M. Recent insights into stearoyl-CoA desaturase-1. *Curr Opin Lipidol*. 2003;14(3):255–261.

30. Pujol A, et al. Late onset neurological phenotype of the X-ALD gene inactivation in mice: a mouse model for adrenomyeloneuropathy. *Hum Mol Genet*. 2002;11(5):499–505.

31. Dumser M, et al. Lack of adrenoleukodystrophy protein enhances oligodendrocyte disturbance and microglia activation in mice with combined Abcd1/Mag deficiency. *Acta Neuropathol*. 2007;114(6):573–586.

32. Strachan LR, et al. A zebrafish model of X-linked adrenoleukodystrophy recapitulates key disease features and demonstrates a developmental requirement for abcd1 in oligodendrocyte patterning and myelination. *Hum Mol Genet*. 2017;26(18):3600–3614.

33. Hsieh SL, et al. cDNA nucleotide sequence coding for stearoyl-CoA desaturase and its expression in the zebrafish (Danio rerio) embryo. *Mol Reprod Dev*. 2003;66(4):325–333.

34. Bhandari S, et al. The fatty acid chain elongase, Elovl1, is required for kidney and swim bladder development during zebrafish embryogenesis. *Organogenesis*. 2016;12(2):78–93.

35. Konantz M, et al. Modeling hematopoietic disorders in zebrafish. *Dis Model Mech*. 2019;12(9):dmm040360.

36. Cassar S, et al. Use of zebrafish in drug discovery toxicology. *Chem Res Toxicol*. 2020;33(1):95–118.

37. Lam PY, et al. Cyp1 inhibition prevents doxorubicin-induced cardiomyopathy in a zebrafish heart-failure model. *Chembiochem*. 2020;21(13):1905–1910.

38. Schrezenmeier E, Dörner T. Mechanisms of action of hydroxychloroquine and chloroquine: implications for rheumatology. *Nat Rev Rheumatol*. 2020;16(3):155–166.

39. Howe K, et al. The zebrafish reference genome sequence and its relationship to the human genome. *Nature*. 2013;496(7446):498–503.

40. Jao LE, et al. Efficient multiplex biallelic zebrafish genome editing using a CRISPR nuclease system. *Proc Natl Acad Sci U S A*. 2013;110(34):13904–13909.

41. Kemp S, et al. Elongation of very long-chain fatty acids is enhanced in X-linked adrenoleukodystrophy. *Mol Genet Metab*. 2005;84(2):144–151.

42. Valianpour F, et al. Analysis of very long-chain fatty acids using electrospray ionization mass spectrometry. *Mol Genet Metab*. 2003;79(3):189–196.

43. Janikiewicz J, et al. Inhibition of SCD1 impairs palmitate-derived autophagy at the step of autophagosome-lysosome fusion in pancreatic β-cells. *J Lipid Res*. 2015;56(10):1901–1911.

44. Zhang Y, et al. Liver X receptor agonist TO-901317 upregulates SCD1 expression in renal proximal straight tubule. *Am J Physiol Renal Physiol*. 2006;290(5):F1065–F1073.

45. Igarashi M, et al. Brain gangliosides in adrenoleukodystrophy. *J Neurochem*. 1976;27(1):327–328.

46. Theda C, et al. Phospholipids in X-linked adrenoleukodystrophy white matter: fatty acid abnormalities before the onset of demyelination. *J Neurol Sci*. 1992;110(1–2):195–204.

47. Hubbard WC, et al. Newborn screening for X-linked adrenoleukodystrophy (X-ALD): validation of a combined liquid chromatography-tandem mass spectrometric (LC-MS/MS) method. *Mol Genet Metab*. 2009;97(3):212–220.

48. Barendsen RW, et al. Adrenoleukodystrophy newborn screening in the Netherlands (SCAN Study): the X-factor. *Front Cell Dev Biol*. 2020;8:499.

49. Jaspers YRJ, et al. Comparison of the diagnostic performance of C26:0-lysophosphatidylcholine and very long-chain fatty acids analysis for peroxisomal disorders. *Front Cell Dev Biol*. 2020;8:690.

50. Yoshida H, et al. XBP1 mRNA is induced by ATF6 and spliced by IRE1 in response to ER stress to produce a highly active transcription factor. *Cell*. 2001;107(7):881–891.

51. Ho JK, et al. Interactions of a very long chain fatty acid with model membranes and serum albumin. Implications for the pathogenesis of adrenoleukodystrophy. *J Clin Invest*. 1995;96(3):1455–1463.

52. Vargas CR, et al. Evidence that oxidative stress is increased in patients with X-linked adrenoleukodystrophy. *Biochim Biophys Acta*. 2004;1688(1):26–32.

53. Collins JL, et al. Identification of a nonsteroidal liver X receptor agonist through parallel array synthesis of tertiary amines. *J Med Chem*. 2002;45(10):1963–1966.

54. DiBlasio-Smith EA, et al. Discovery and implementation of transcriptional biomarkers of synthetic LXR agonists in peripheral blood cells. *J Transl Med*. 2008;6:59.

55. Potze L, et al. Betulinic acid induces a novel cell death pathway that depends on cardiolipin modification. *Oncogene*. 2016;35(4):427–437.

56. Kemp S, et al. Gene redundancy and pharmacological gene therapy: implications for X-linked adrenoleukodystrophy. *Nat Med*. 1998;4(11):1261–1268.

57. Rizzo WB, et al. Adrenoleukodystrophy: oleic acid lowers fibroblast saturated C22-26 fatty acids. *Neurology*. 1986;36(3):357–361.

58. Gong Y, et al. Intrathecal adeno-associated viral vector-mediated gene delivery for adrenomyeloneuropathy. *Hum Gene Ther*. 2019;30(5):544–555.

59. Eichler F, et al. Hematopoietic stem-cell gene therapy for cerebral adrenoleukodystrophy. *N Engl J Med*. 2017;377(17):1630–1638.

60. Madison KC. Barrier function of the skin: "la raison d'être" of the epidermis. *J Invest Dermatol*. 2003;121(2):231–241.

61. Helder RWJ, et al. The effects of LXR agonist T0901317 and LXR antagonist GSK2033 on morphogenesis and lipid properties in full thickness skin models. *Biochim Biophys Acta Mol Cell Biol Lipids*. 2020;1865(2):158546.

62. Sassa T, et al. Impaired epidermal permeability barrier in mice lacking elovl1, the gene responsible for very-long-chain fatty acid production. *Mol Cell Biol*. 2013;33(14):2787–2796.

63. Katz A, et al. Safety, pharmacokinetics, and pharmacodynamics of single doses of LXR-623, a novel liver X-receptor agonist, in healthy participants. *J Clin Pharmacol*. 2009;49(6):643–649.

64. Huffnagel IC, et al. Comparison of C26:0-carnitine and C26:0-lysophosphatidylcholine as diagnostic markers in dried blood spots from newborns and patients with adrenoleukodystrophy. *Mol Genet Metab*. 2017;122(4):209–215.

65. Khan M, et al. Plasmalogen deficiency in cerebral adrenoleukodystrophy and its modulation by lovastatin. *J Neurochem*. 2008;106(4):1766–1779.

66. Iwai T, et al. Stearoyl-CoA desaturase-1 protects cells against lipotoxicity-mediated apoptosis in proximal tubular cells. *Int J Mol Sci*. 2016;17(11):1868.

67. Paterniti I, et al. Liver X receptor agonist treatment regulates inflammatory response after spinal cord trauma. *J Neurochem*. 2010;112(3):611–624.

68. Wu CH, et al. Treatment with TO901317, a synthetic liver X receptor agonist, reduces brain damage and attenuates neuroinflammation in experimental intracerebral hemorrhage. *J Neuroinflammation*. 2016;13(1):62.

69. Sohrabi Y, et al. LXR activation induces a proinflammatory trained innate immunity-phenotype in human monocytes. *Front Immunol*.

2020;11:353.

70. Ménégaut L, et al. Interplay between liver X receptor and hypoxia inducible factor 1α potentiates interleukin-1β production in human macrophages. *Cell Rep*. 2020;31(7):107665.

71. Jang J, et al. 25-hydroxycholesterol contributes to cerebral inflammation of X-linked adrenoleukodystrophy through activation of the NLRP3 inflammasome. *Nat Commun*. 2016;7:13129.

72. Shackleford GG, et al. Liver X receptors differentially modulate central myelin gene mRNA levels in a region-, age- and isoform-specific manner. *J Steroid Biochem Mol Biol*. 2017;169:61–68.

73. Li J, et al. Lipid desaturation is a metabolic marker and therapeutic target of ovarian cancer stem cells. *Cell Stem Cell*. 2017;20(3):303–314.

74. Fretts AM, et al. Associations of circulating very-long-chain saturated fatty acids and incident type 2 diabetes: a pooled analysis of prospective cohort studies. *Am J Clin Nutr*. 2019;109(4):1216–1223.

75. Lemaitre RN, et al. Circulating very long-chain saturated fatty acids and heart failure: the cardiovascular health study. *J Am Heart Assoc*. 2018;7(21):e010019.

76. Melles RB, Marmor MF. The risk of toxic retinopathy in patients on long-term hydroxychloroquine therapy. *JAMA Ophthalmol*. 2014;132(12):1453–1460.

77. Gevers S, et al. Safety considerations for chloroquine and hydroxychloroquine in the treatment of COVID-19. *Clin Microbiol Infect*. 2020;26(9):1276–1277.

78. Schultz JR, et al. Role of LXRs in control of lipogenesis. *Genes Dev*. 2000;14(22):2831–2838.

79. Baranowski M. Biological role of liver X receptors. *J Physiol Pharmacol*. 2008;59 Suppl 7:31–55.

80. Sukardi H, et al. Liver X receptor agonist T0901317 induced liver perturbation in zebrafish: histological, gene set enrichment and expression analyses. *Biochim Biophys Acta*. 2012;1820(1):33–43.

81. Fessler MB. The challenges and promise of targeting the liver X receptors for treatment of inflammatory disease. *Pharmacol Ther*. 2018;181:1–12.

82. Xing L, et al. Rapid and efficient zebrafish genotyping using PCR with high-resolution melt analysis. *J Vis Exp*. 2014;(84):e51138.

83. Forss-Petter S, et al. Targeted inactivation of the X-linked adrenoleukodystrophy gene in mice. *J Neurosci Res*. 1997;50(5):829–843.

84. Bedossa P, et al. Histopathological algorithm and scoring system for evaluation of liver lesions in morbidly obese patients. *Hepatology*. 2012;56(5):1751–1759.

85. Molenaars M, et al. A conserved mito-cytosolic translational balance links two longevity pathways. *Cell Metab*. 2020;31(3):549–563.e7.

86. Engelen M, et al. Cholesterol-deprivation increases mono-unsaturated very-long-chain fatty acids in skin fibroblasts from patients with X-linked adrenoleukodystrophy. *Biochim Biophys Acta*. 2008;1781(3):105–111.

87. Kemp S, et al. Method for measurement of peroxisomal very-long-chain fatty acid beta-oxidation in human skin fibroblasts using stable-isotope-labeled tetracosanoic acid. *Clin Chem*. 2004;50(10):1824–1826.

88. van de Beek MC, et al. Method for measurement of peroxisomal very long-chain fatty acid beta-oxidation and de novo C26:0 synthesis activity in living cells using stable-isotope labeled docosanoic acid. *Methods Mol Biol*. 2017;1595:45–54.